Diplomarbeit

Inundation–Desiccation State Prediction for Salt Pans in the Western Pannonian Basin using Remote Sensing, Groundwater, and Meteorological Data

zur Erlangung des akademischen Grades
Diplom-Ingenieur

im Rahmen des Studiums
Geodäsie und Geoinformation

eingereicht von

Henri Schauer, B.Sc.
Matr.Nr.: 12033340

ausgeführt am
Department für Geodäsie und Geoinformation
der **Fakultät für Mathematik und Geoinformation**
der **Technischen Universität Wien**

unter der Betreuung von
Univ.Prof. Dr.rer.nat. Wouter Dorigo
unter Mitwirkung von
Dr.rer.nat. Stefan Schlaffer; Emanuel Büechi, M.Sc.

Wien, am 31. Oktober 2023

(Unterschrift Verfasser) (Unterschrift Betreuer)

Declaration

I hereby declare that I have written this thesis by myself without any help or assistance of others. External literature used to clarify the content or provided data sources are fully cited. All mentioned information is in accordance with fact or truth up to my knowledge.

Vienna, on October 31, 2023

(Signature author)

Abstract

Salt pans are unique wetland ecosystems. In the Austrian Seewinkel region, salt pans are in an increasingly vulnerable state due to groundwater drainage and heightened climatic pressures. It is crucial to model how seasonal and long-term hydrological and climatological variations affect the salt pan dynamics in Seewinkel, yet a comprehensive understanding of the driving processes is lacking. The goal of this study is to develop random forest machine learning models driven by hydrological and meteorological data that allow us to predict in early spring (March) of each year the inundation state in the subsequent summer and fall. We utilize Earth observation data from Landsat 5 (L5), 8 (L8), and 9 (L9) to derive the time series of the inundation state for 34 salt pans for the period 1984–2022. Furthermore, we demonstrate that the groundwater level observed in March is the strongest predictor of the salt pan inundation state in summer and fall. Utilizing local groundwater data yields a Matthews correlation coefficient of 0.59. Models using globally available meteorological data, either instead of or in addition to groundwater data, provide comparable results. This allows the global transfer of the approach to comparable ecosystems where no in situ data are available.

Preface

This master thesis builds on a paper that was recently published in MDPI *Remote Sensing* journal: Schauer et al. (2023). The submitted paper is lead-authored by me, goes under the same title as this thesis and has been published on the 22 September 2023. The co-authors of the submitted paper are: Stefan Schlaffer, Emanuel Bueechi, and Wouter Dorigo. I contributed to the paper by providing the predictor data sets, by analyzing the predictor and target datasets, by coding the machine learning models, by doing the analysis, by plotting and by drafting the manuscript except for Section 2.2, Section 3.1.1 and the first paragraph and Table 3 of Section 4.1 of Schauer et al. (2023). These sections are not part of this master thesis to ensure complete independence of this thesis from work that has been done by anyone but myself. Generally, the derivation of the water extent time series of the salt pans was performed by Stefan Schlaffer (see indication in Section 2.2, Section 3.1.4 and Section 4.1 (first sentence) of this thesis). Here, the exact methods used to derive the time series are not presented (see Section 2.2, Section 3.1.1 of Schauer et al. (2023)), whereas a more general overview over remote sensing of wetlands, and salt pans in particular, will be given.

For this master thesis the paper was extended by providing more theoretical background with a focus on the methods. Special focus is put on salt pans and the role of earth observation in the quantification of salt pan water extent. Furthermore, the theory behind Random Forest machine learning models is explained. All sections except for Sections 1.1, 3.1 (the paragraph until Section 3.1.1), 3.1.1, 3.1.2, 3.1.3, and 3.2.2 are directly adopted from Schauer et al. (2023). Other exceptions are Section 2.2, Section 3.1.4 and Section 4.1 (first sentence) that are used to indicate work done by Stefan Schlaffer. All figures except for Figure 3.1 are adopted from Schauer et al. (2023). The abstract was also adopted from Schauer et al. (2023).

Contents

List of Figures

List of Tables

1. Introduction

Salt pans are a special type of terrestrial wetlands, which are formed in relation to arid climates, topographic depressions, and salt-rich groundwater (Lowenstein et al. 1985; Shaw et al. 2011). They can be defined as "(...) arid zone basins (...), subject to ephemeral surface water inundation of variable periodicity and extent" (Shaw et al. 2011). Saline lakes, such as salt pans, are of vital importance for biodiversity and water management (Shaw et al. 2011; Leemans et al. 2003); however, at the global scale, their number is declining mainly due to direct human intervention in their hydrology and climate change (Wurtsbaugh et al. 2017; W. D. Williams 2004). Although global data on salt pans are missing (Safaee et al. 2020), many case studies suggest a global trend toward salt pan degradation and decline (Shaw et al. 2011; W. D. Williams 2004; Wasserman et al. 2022; Nayak et al. 1989; Picado et al. 2009; Silva et al. 2022). These trends also apply to the salt pans in Seewinkel in eastern Austria (Herzig 2020; Boros et al. 2013), where key regional ecosystem functions are under threat. The lives of, among others, halophytes (Albert et al. 2020), amphibians, reptiles (Krachler et al. 2012; Cabela et al. 2001), and birds (Dvorak et al. 2017; Dvorak et al. 2020) depend on these wetlands. Halophytes, such as communities of *Puccinellio-Salicornietea*, require a high groundwater level facilitating capillary rise to ensure their water supply (Albert et al. 2020). Birds, such as the kentish plover (*Charadrius alexandrinus*), use high water levels in spring (for hatching (Dvorak et al. 2016)) and summer (Dvorak et al. 2020), as do amphibians and reptiles (Krachler et al. 2012; Cabela et al. 2001). In Central Europe, such ecosystems can only be found in the Pannonian Basin (Boros et al. 2017) due to the unique tectonic conditions in the region (Krachler et al. 2000). In recent years, processes such as eutrophication, paludification, siltation, overgrowth with vegetation, fragmentation, long-term drying, and in consequence, habitat loss, have accelerated (Zimmermann-Timm et al. 2021; Horváth et al. 2019). These are largely connected to excessive groundwater drainage for land use change (Zimmermann-Timm et al. 2021; Mitter et al. 2021). The potential impact of climate change on the salt pans in Seewinkel is not yet fully understood (Mitter et al. 2021), although small, geographically isolated wetlands reportedly react rather quickly to meteorological forcing (M. K. Vanderhoof et al. 2018).

The salt pans in the Seewinkel region follow the salt pan cycle (Lowenstein et al. 1985), in which the dry basin is the default, central, and recurrent moment, which is alternated by its opposite state: the varying presence of water (Lowenstein et al. 1985; Sharma et al. 2021). In summer, high evaporation rates in combination with an interruption of groundwater supply tend to outweigh precipitation (Krachler et al. 2012) leading to salt pan desiccation. Especially

during late winter and early spring (Zimmermann-Timm et al. 2021), low evaporation rates allow precipitation combined with an increased contribution of groundwater to fill the basins. Wind contributes to important ecosystem processes as it influences evaporation rates and drives the mixing of water when the salt pan is inundated (Zimmermann-Timm et al. 2021). It also strengthens capillary rise and blows out inorganic sediments from the salt pan basins during periods of desiccation (Krachler et al. 2000). Salt pans in poor hydrological conditions lose additional water by surface water infiltrating into deeper soil layers (Krachler et al. 2012). Thus, monitoring and predicting both the long-term and short-term variability of surface water occurrence in the Seewinkel salt pans is needed to assess ecosystem change and their resilience.

Wetland hydroperiod (D. D. Williams 2006), a key characteristic and ecological indicator of intermittent wetlands, such as salt pans (Nhiwatiwa et al. 2017; Boros et al. 2017), can be characterized by means of water height (WH), water extent (WE), or water volume (WV) (Turak et al. 2017; Shaw et al. 2011; Foti et al. 2012). WH derived from in situ water level gauges offers the most reliable and temporally frequent source of information. However, water gauges provide merely vertical, locally tied measurements and are costly to install and maintain. Especially for salt pans, the water level gauge must be positioned at the deepest point due to increased drying towards the edges. In many regions of the world, long-term, automatic in situ measurements are not widely available, as is also the case for the Seewinkel region (web address: `https://wasser.bgld.gv.at/hydrographie/die-seen` and `https://ehyd.gv.at/` (accessed on 14 August 2023)).

WE is especially suited for studying the inundation state of the salt pans due to their shallow topography so that small changes in water volume cause substantial changes in water surface area. WE can be reliably retrieved from Earth observation (EO) satellite data that provide global, freely available information of high spatial and sufficient temporal resolution (Hess et al. 2003; Reschke et al. 2012). Multispectral imagery has proven to be suitable for studying salt pans because of the high reflectivity of exposed salt surfaces and the absorption of infrared radiation by water surfaces (Safaee et al. 2020). Although commonly suffering from cloud cover, multispectral observations are less affected by wind than radar systems (Krzepek et al. 2022; Kseňak et al. 2022; Bartsch et al. 2012), which have been widely used to monitor wetlands (Schlaffer et al. 2022; Hess et al. 2003; Prigent et al. 2007; Reschke et al. 2012). Most studies use data from the moderate resolution imaging spectroradiometer (MODIS) (Justice et al. 1998) or a series of the Landsat missions, which together cover an observation period of nearly 50 years (Wulder et al. 2019). Examples of global satellite-derived WE products are the global surface water (GSW) product (Pekel et al. 2016) and the dynamic surface water extent product (Jones 2019). Additionally, continental-scale products exist (Sheng et al. 2016). These large-scale products include data on salt pans (Figure 1.1); however, they are often inaccurate for small-size ecosystems, such as those encountered in Seewinkel (Pekel et al. 2016). Local case studies using remote sensing to derive WE and inundation states are numerous (Heintzman et al. 2017; Lefebvre et al. 2019; Castañeda et al. 2005; Bowen et al. 2017; Chiloane et al. 2020; Bryant et al. 2002; Chew et al. 2020; H. Li et al. 2019; Schlaffer et al. 2016).

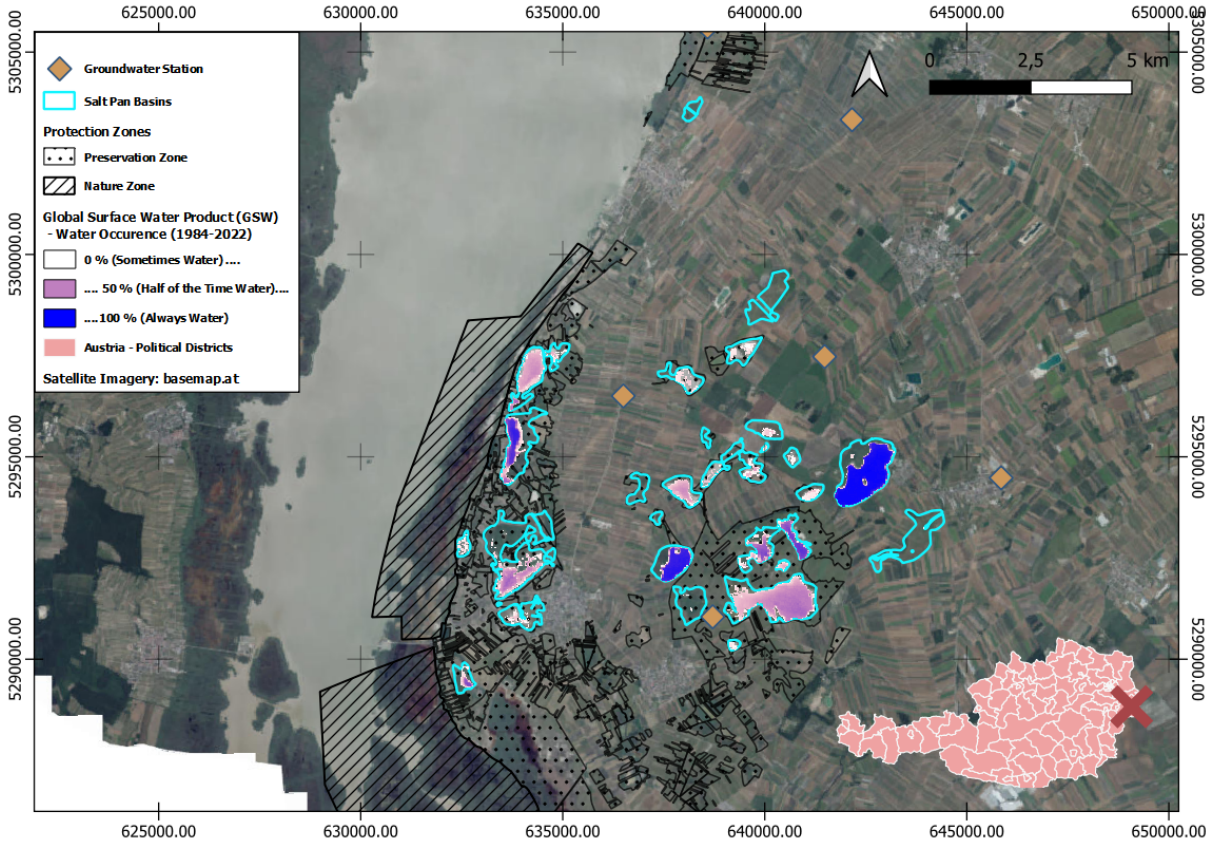

Fig. 1.1: Location of Seewinkel in Eastern Austria. Outlines of salt pan basins were provided by Lake Neusiedl—Seewinkel National Park administration (Nationalpark Neusiedler See - Seewinkel 2022). Additionally, the groundwater stations used in the study are marked. The salt pans are colored based on the water occurrence product of the Global Surface Water (GSW) data set (Pekel et al. 2016). The basemap stems from basemap.at (web address: `https://basemap.at/` (accessed on 14 August 2023)). The coordinate reference system is the MGI/Austria GK M34 (EPSG:31259; web address: `https://epsg.io/31259` (accessed on 14 August 2023)). The map inset shows the location of the study area (marked with an X) within Austria.

Several modeling approaches exist that link various drivers to salt pan hydrological properties. Traditional hydrological modeling (Jajarmizadeh 2012; Z. Liu et al. 2017; G. Liu et al. 2011) applied to wetlands depends on a certain quantity and quality of data for parameterization, which often hampers their spatial transferability to regions where these data are not available (Blöschl et al. 1995; Patil et al. 2015; Chouaib et al. 2018; C. Z. Li et al. 2012; Yang et al. 2022). Stochastic modeling has long been recognized as a vital alternative to process-based modeling (Farmer et al. 2016). A number of studies have focused on summarizing past, present, and perspective machine learning (ML) methodology in estimating different hydrological variables (C. Shen et al. 2021; Nearing et al. 2021; Lange et al. 2020; Mosaffa et al. 2022; Osman et al. 2022; Afrifa et al. 2022; Ahmadi et al. 2022; Ardabili et al. 2020; Zounemat-Kermani et al. 2021; T. Xu et al. 2021; Papacharalampous et al. 2022), such as groundwater (Osman et al. 2022; Afrifa et al. 2022; Ahmadi et al. 2022). Conventional ML models, such as the random forest (RF)

approach (Breiman 2001; Tyralis et al. 2019), have been the most commonly used concepts for modeling hydrological variables (T. Xu et al. 2021; Papacharalampous et al. 2022). They encompass the advantage of being well explored, non-parametric, often robust estimators that, in many cases, offer extensive algorithmic options for model interpretation (T. Xu et al. 2021). Hybrid models (Kraft et al. 2022; Fahimi et al. 2017; Nourani et al. 2014; Khandelwal et al. 2020) and deep learning models (Sit et al. 2020) have only recently gained attention in hydrological research (Khandelwal et al. 2020; Sit et al. 2020). Hybrid models are meant to incorporate the advantages of traditional hydrological modeling and ML modeling (Kraft et al. 2022; Fahimi et al. 2017; Nourani et al. 2014; Khandelwal et al. 2020). Although fit for complex pattern recognition tasks, deep learning models typically require large amounts of data for model training (LeCun et al. 2015; Sit et al. 2020) and are harder to interpret (Chakraborty et al. 2017).

Advances in ML (T. Xu et al. 2021; Papacharalampous et al. 2022) have boosted the relevance of stochastic modeling for predicting lake WH (Wee et al. 2021; Hussaini et al. 2020; S. Zhu et al. 2020; B. Li et al. 2016; Choi et al. 2020). Past research in modeling wetland inundation dynamics using ML methods is often restricted to using in situ measurements for identifying the presence of water (Cartwright et al. 2022; Riley et al. 2023). Greater data availability provided by EO (Dorigo et al. 2021; Sogno et al. 2022; Pekel et al. 2016) has contributed to studies utilizing WE for modeling wetlands, although, to our knowledge, not for salt pans and in different temporal resolutions. The monthly inundation state of freshwater playas in the Great Plains of North America has been modeled on a large spatial scale using a monthly global water extent product based on Landsat (Pekel et al. 2016) and climate and land cover data (Solvik et al. 2021). Inundation patterns in the Darling River Floodplain, Australia, were modeled using Landsat data and topography, meteorological, and hydrological data (Shaeri Karimi et al. 2019). Satellite-derived WE (lake surface area) of Lake Gregory, Australia's salt lake, has been modeled using ML with precipitation and temperature as predictors (Soltani et al. 2020). Quantification of wetland permanence of four water body permanence classes in the Prairie Pothole Region, although not carried out for salt pans, was executed by Daniel et al. (2022), who, in addition to climate and land cover, introduced features based on topography to ML modeling. Various ML models were used for the mentioned studies. Solvik et al. (2021) used a long short-term memory neural network, Shaeri Karimi et al. (2019) used RF, Soltani et al. (2020) applied a generalized group method of data handling, and Daniel et al. (2022) used extreme gradient boosting techniques.

1.1 Objective of this thesis

The goal of this master thesis is to build ML models to predict the inundation–desiccation state of 34 salt pans in Seewinkel, Austria from 1984-2022. Three models combine the yearly salt pan inundation–desiccation state during July, August, September, or October (JASO) retrieved from the Landsat satellite archive (Wulder et al. 2016; Wulder et al. 2019) as model target with either in situ groundwater measurements, meteorological data from the ERA5-Land global reanalysis (Muñoz-Sabater et al. 2021) or both as predictors. In order to understand the

influence of changing meteorological patterns and groundwater withdrawal on salt pan dynamics, explainable artificial intelligence (Gunning et al. 2019) is utilized.

This master thesis is structured the following: in chapter 2 the study area and the data sets used to model salt pan inundation state are presented. Chapter 3 focuses on the derivation of salt pan WE by means of remote sensing with a focus on multispectral remote sensing and it explains the concept of Random Forest algorithms. Chapter 3 additionally provides a detailed description of the model setup, feature importance and evaluation metrics. Chapter 4 presents the results, while Chapter 5 discusses the results with a focus on the model assumptions, predictors, targets, model error, and model transferability. Finally, in chapter 6, conclusions are drawn and an outlook is provided.

2. Materials

2.1 Study area

The study area is located in the Lake Neusiedl—Seewinkel National Park (Figure 1.1). Salt pans in Seewinkel are steppe wetlands (Krachler et al. 2012) and mostly relicts of the Würm glaciation (Draganits et al. 2022; Häusler 2007). Their size ranges between 0.03 km^2 and 1.5 km^2 (based on the data collected in the scope of this study). The salt pans are highly heterogeneous in their hydrological and ecological condition (Krachler et al. 2012; Kirschner et al. 2007). Due to various causes, the number of salt pans in Seewinkel has decreased from 139 in the year 1855 to about 59 ecologically intact specimens in 2012 (Krachler et al. 2012). Historically, the landscape has been subject to strong economic utilization, most notably through the intensification and expansion of agricultural practices since the 1960s (Draganits et al. 2022) and because of tourism (Krachler et al. 2012). A process referred to as "drying from beneath" (Krachler et al. 2000) has been identified as the main driver behind "dying salt pans" (Krachler et al. 2012), although diverging theories exist (Häusler 2020; Häusler 2007). Due to human-induced groundwater drainage, the capillary rise is disrupted starting at a depth to groundwater of approximately 70 cm (Zimmermann-Timm et al. 2021). This finally results in the failure of the water retention capacity of the salt pans and desalinization (Zimmermann-Timm et al. 2021). Some salt pans tend to be naturally filled with water all year (type: 'naturally perennial'), and some artificially hold water over the whole year (type: 'artificially perennial'). Others tend to desiccate over continuous periods of time (type: 'periodically filled') (Krachler et al. 2012).

The climate in Seewinkel can be classified as Dfb-climate (warm-summer humid continental; based on monthly ERA5-Land data from 1984 to 2022; Köppen-Geiger climate classification (Köppen 2011)). The total annual potential evaporation (E_{pot}) is 602 mm (1978–2010; (Soja et al. 2013)), the total annual precipitation (P) is 556 mm (1971–2020; (Hackl et al. 2023)), and the annual mean 2 m temperature (T) is 11.1 °C (1971–2020; (Hackl et al. 2023)). P is highest from May to September and lowest from October to April (based on monthly ERA5-Land from 1984 to 2022; verified via Crocetti et al. (2020)). While there is research on the impact of climate change on Lake Neusiedl (Hackl et al. 2023; Soja et al. 2013; Tolotti et al. 2021; Eitzinger et al. 2005), it remains unclear whether climate change currently affects the salt pans in Seewinkel (Mitter et al. 2021). Most scenarios (Representative Concentration Pathway (RCP) 4.5 and RCP 8.5) for the Austrian state of Burgenland predict a significant increase in temperature for all seasons, whereas a slight increase in mean annual precipitation is expected together with a significant increase

(+33%) in winter precipitation in the distant future (RCP 8.5) (Burgenland 2016). Based on climate scenarios, it is estimated that the return period of moderate and extreme droughts will decrease in lowland Austria over the course of the 21st century (Haslinger et al. 2023), suggesting greater pressure on vulnerable wetland ecosystems in the future.

2.2 Target data

The WE time series of 34 salt pans in Seewinkel were provided by Stefan Schlaffer and are explained in Schauer et al. (2023), Section 2.2.

2.3 Predictor data

2.3.1 Predictor selection

The selected features relate to the main drivers of salt pan variability, i.e., groundwater, precipitation, temperature, and evaporation (Table 2.1). They were narrowed down from a larger set of potential drivers based on the literature on wetlands and salt pan modeling in general, as well as the salt pans in Seewinkel, in particular (Lowenstein et al. 1985). For example, topography, a feature proposed by Daniel et al. (2022), was excluded as a predictor since the variation between salt pan basins is likely to be minimal (based on a local digital elevation model (DEM) (web address: `https://geodaten.bgld.gv.at/de/downloads/hoehenmodelle-orthofotos.html` (accessed on 14 August 2023))). Information on anthropogenic drivers in sufficient resolution, e.g., well extraction amounts or channel discharge, was not available (RH 2020).

WE in spring is expected to have a major impact on inundation state estimates in summer (Zimmermann-Timm et al. 2021). However, we did not include WE as a predictor for the following reasons: First, its inclusion potentially results in overshadowing other predictors. Although possibly improving model performance, this would limit model interpretability and ecosystem understanding. Second, natural spring WE is the result of the underlying processes steered by groundwater, precipitation, temperature, and evaporation. Hence, WE information is implicitly included in the nine predictors used in this study.

To account for interannual variability in hydrological and meteorological conditions, we applied various integration periods to the selected predictors. However, the overall focus is on integration over 12 months as this period covers the entire time since the last prediction was made. Other integration periods span 6 months, whereas the SGI is a continuous variable, as indicated in Table 2.1. To detect trends in the features, we applied the Mann-Kendall test (Hamed et al. 1998) to the nine predictors. We abstained from feature selection methods (Jović et al. 2015) as we wanted to obtain information on feature importance and partial dependencies on all introduced predictors. Importantly, our sample size is expected to be large enough with respect to the maximum number of features (nine features for the combined model), hence decreasing the likelihood of overfitting (Sima et al. 2006).

Tab. 2.1: The nine predictors used for modeling inundation state are divided into meteorology and hydrology. Furthermore, the relation to the salt pan cycle is explained, and additional information is provided.

Field	Variable [Unit]	Derived Predictor [Unit] (Abbrev.)	Integ. Period	Relation to Salt Pan Cycle	Data Source
Hydrology	Groundwater [m.a.s.l.]	Anomalies [unitless] (GW Anom.)	12 m.	Groundwater is of key importance for salt pan water abundance in Seewinkel (Zimmermann-Timm et al. 2021) Short-term and especially long-term groundwater depletion leads to salt pan degradation (Krachler 2007)	Austrian eHyd portal
		SGI [unitless] (SGI)	Cont.	The Standardized Groundwater Index can serve as a robust estimation of groundwater drought (Bloomfield et al. 2013; Turkeltaub et al. 2023) Groundwater drought in March influences the salt pan water extent in spring and therefore the inundation state in summer	
		Level ratio [unitless] (GW level ratio)	Oct./March (6 m.)	Fall-winter groundwater level ratio is closely connected to regional precipitation during that time (Hughes et al. 2021) The level ratio stands in relation to salt pan water extent in spring (Krachler et al. 2012)	
Meteorology	Temperature [°C]	Anomalies [unitless] (T Anom.)	12 m.	Higher temperature increases water temperature (Oroud 1999; Oroud 2001; T. Liu et al. 2017; Zimmermann-Timm et al. 2021) Higher summer temperature increases evaporation and therefore the number of drying events (Krachler et al. 2012) Higher temperatures in winter decrease spring water extent (Krachler et al. 2000)	ERA5-Land (Muñoz-Sabater et al. 2021), DOI: 10.24381/cds.68d2bb30
		Numb. of days above 25 °C [days]	12 m.	The number of days above 25 °C is connected to heatwaves and extensive evaporation (WMO 2017)	
	Evaporation [mm]	Anomalies [unitless] (Epot Anom.)	12 m.	Evaporation leads to salt pan concentration and desiccation (Lowenstein et al. 1985; Bloch et al. 1951)	
	Precipitation [mm]	Anomalies [unitless] (P Anom.)	12 m.	Precipitation leads to salt pan filling (Lowenstein et al. 1985) Precipitation leads to eluviation of the saliferous horizon (Krachler et al. 2000) Precipitation as observed over a 12-month period is related to hydrological drought (Vicente-Serrano et al. 2010)	
		SPI 6 [unitless]	6 m.	Standardized Precipitation Index 6 is connected to medium-term precipitation patterns and agricultural drought (McKee et al. 1993; Kumar et al. 2016)	
		SPI 24 [unitless]	24 m.	Standardized Precipitation Index 24 is connected to long-term precipitation patterns and hydrological/socioeconomic drought (Vicente-Serrano et al. 2010; McKee et al. 1993; Kumar et al. 2016; Secci et al. 2021)	

2.3.1.1 Groundwater level

Seewinkel is equipped with 84 groundwater gauges located in relative proximity to the salt pans. Of these, only six provide continuous observations throughout the time span covered by the Landsat observations and could thus be used for our study (i.e., stations 306043, 319418, 316174, 305755, 305813, and 319426). The point-based data are provided natively as monthly means through eHyd (web address: `https://ehyd.gv.at/` (accessed on 14 August 2023)). First, we derived the mean monthly groundwater level of the six stations. We then calculated the groundwater anomalies to exclude long-term climatology. This was completed by subtracting the mean seasonal component from the original time series (Bueechi et al. 2023; Papagiannopoulou et al. 2017):

$$A_t = D_t - C_t, \tag{2.1}$$

where A_t is the anomaly at time t, D_t is the monthly averaged values at time t, and C_t is the long-term seasonal climatology. C_t was calculated by averaging groundwater levels per month for the entire reference period from 1984 to 2022. Finally, we calculated the 12-month average of the time series between April (previous year) and March (current year) to derive presummer season groundwater anomalies for each year. All of these steps were executed with the Python packages numpy (Harris et al. 2020) and pandas (team 2023). We decided not to apply further detrending to the anomalies to inform the model about long-term environmental changes (e.g., introduced by human management).

Other predictors that were derived are the Standardized Groundwater Index (SGI) in March of each year and the October/March groundwater level ratio (Bloomfield et al. 2013). The SGI is the only predictor with a continuous accumulation period and is based on a non-parametric normal scores transform of the groundwater level data for each calendar month (Bloomfield et al. 2013). It represents information on the groundwater level, not as an average over 12 months, but as derived in March. The SGI was also calculated based on the monthly groundwater values averaged across all six stations. The calculation was executed through the Python package pastas (Collenteur et al. 2019). The groundwater level ratio was calculated as the ratio of the groundwater level in March (the time of prediction and typically the time of year of the groundwater level maximum (Zimmermann-Timm et al. 2021)) divided by the level in October of the previous year (approx. the lowest level (Zimmermann-Timm et al. 2021)). It serves as a proxy for groundwater recharge during winter.

2.3.1.2 ERA5-Land meteorology

The ERA5-Land reanalysis (Muñoz-Sabater et al. 2021) is aimed at land applications. It has the following main characteristics: the data from ERA5-Land offers a high spatial (ca. 9 km × 9 km) and temporal resolution, global availability, and temporal coverage dating back to the 1950s, thus, overlapping with Landsat retrieval periods (Bandhauer et al. 2022; Lavers et al. 2022; Hersbach et al. 2020; Bell et al. 2021). Three variables were used: the total precipitation P, the potential

evaporation E_{pot}, and the 2 m temperature T. The E_{pot} in ERA5-Land is higher than the Pannonian average of 600-800 mm per year (Nistor et al. 2017) as the E_{pot} is often overestimated because of representing open water evaporation (Muñoz-Sabater et al. 2021). We used the ERA5-Land monthly averaged data from 1950 to the present (DOI: 10.24381/cds.68d2bb30) for the calculation of nearly all meteorological predictors. Only the number of days in a year with a maximum temperature above 25 °C was derived from hourly 2 m temperature data based on the ERA5-Land hourly data (DOI: 10.24381/cds.e2161bac).

First, the seven pixels covering the study area were combined by spatial averaging for each variable. Preprocessing of the ERA5-Land variables was performed in accordance with Equation (2.1) and the Python packages numpy (Harris et al. 2020) and pandas (team 2023). Subsequently, a 12-month average was performed in the case of T and a 12-month summation in the cases of P and E_{pot}. For the same reason mentioned in Section 2.3.1.1, detrending was not performed for these three features either. In addition, we used the ERA5-Land monthly P to compute the drought indicator standardized precipitation index (SPI) over 6 months and 24 months (SPI; (McKee et al. 1993; Cheval 2015)) using the R package SPEI (Vicente-Serrano et al. 2010). The SPI represents the precipitation conditions of a predefined time period in relation to the respective normal values. It builds on the calculation of a normal distribution as in reference (Cheval 2015). Furthermore, the number of days in a year with a maximum temperature above 25 °C was derived.

3. Methods

3.1 Remote sensing of salt pans

Based on the atmospheric windows, two different frequency domains can be considered to acquire high-resolution images of salt pans: the optical domain and the microwave domain (Rees 2012). Both optical imagery (Heintzman et al. 2017; Lefebvre et al. 2019; Castañeda et al. 2005; Bowen et al. 2017; Chiloane et al. 2020; Bryant et al. 2002; H. Li et al. 2019) and microwave imagery (Schlaffer et al. 2022; Hess et al. 2003; Prigent et al. 2007; Reschke et al. 2012; Chew et al. 2020; Schlaffer et al. 2016) have been widely used for water body and soil salinity monitoring. The crucial procedure for deriving the inundation state of salt pans, independent of the wavelength, is pixel-wise recognition of spectral signatures of water and non-water surfaces (Jensen 2007). This is based on the unique physical properties of water, desiccated (saline) surfaces, and the riparian zone surrounding the salt pans (Jensen 2007).

3.1.1 Multispectral remote sensing of salt pans

Multispectral remote sensing data are characterized by their radiometric, spatial, spectral, and temporal resolution (Vijayaraj et al. 2006). The former represents the amount of radiometric information in each pixel, that is, the dynamic range of the total radiance (TR) (level 1 data; represented in bits). Applying radiometric models can help identify whether the radiation stems from the different components of the equation for aquatic environments:

$$L_t = L_p + L_s + L_v + L_b, \tag{3.1}$$

where L_t is the TR, L_p is the radiance from atmospheric scattering (path radiance), L_s is the water surface radiance, L_v is the subsurface volumetric radiance and L_b is the radiance from the bottom of the water body (Jensen (2007); for a more complex formulation see Mustard et al. (2001)). Radiometric corrections based on analytical or empirical models can help isolate terms and therefore provide information on, e.g., the surface component of the TR within a specific pixel or the subsurface volumetric radiance of suspended particulate matter concentrations (Doxaran et al. 2002).

To identify water and non-water pixels, it is useful to treat them not merely as a function of energy (radiometric resolution), but as a function of frequency (spectral resolution) (Wezernak et al. 1976; Jensen 2007). Here, the use of spectral reflectance products (level 2; property of the

material being observed; relative reflection between 0 and 1) instead of TR products is helpful (Bowker 1985). The necessary corrections to allocate spectral radiance to the earth's surface (instead of the atmosphere or measurement geometry) are already included and ensure ease of use (Wulder et al. 2022).

Optical remote sensing is a passive technique that relies on solar radiation (Booysen et al. 2021). It is based on electromagnetic radiation frequencies ranging from 0.3 μm to 15 μm (visible: 0.38 μm to 0.75 μm; near-infrared (NIR): 0.75 μm to 1.4 μm; short-wave infrared (SWIR): 1.4 μm to 3.0 μm) (Kerekes 2008), although there are different spectral subdivisions (Rees 2012). The continuous electromagnetic spectrum is commonly separated into up to 15 bands for multispectral systems and more than 200 bands for hyperspectral systems (Landgrebe 2003; Bioucas-Dias et al. 2013; Jensen 2007). We decided to use the visible, NIR and SWIR bands as baseline, as they work best for discriminating water pixels (which typically appear dark in the image) from non-water pixels (which appear more bright in the image) (Jensen 2007). To retrieve the salt pan water surface extent, it is necessary to differentiate between the two main land surface constituents in and around the salt pan basins, i.e., vegetation and (saline) soil from water. To maximize the contrast between pixels, the unique spectral properties of the constituents are utilized (Figure 3.1). To detect water surfaces, we rely on the property of water as a strong absorber of incident radiation throughout the visible, NIR, and SWIR spectrum. The spectral signatures between different types of soil and vegetation are less distinct (Figure 3.1).

For wavelengths between 0.74 μm and 2.5 μm, clear water absorbs most incident radiation (Figure 3.1; Jensen (2007)). Due to the increased radiant flux of organic and non-organic constituents in some water bodies, Jensen (2007) suggested particular care in the use of the NIR spectral region to discriminate water surfaces from surrounding soil and vegetation. Here, SWIR is reported to be particularly useful (Safaee et al. 2020). Inundated salt pans in Seewinkel exhibit considerable amounts of suspended materials, such as clay (phyllosilicates) in the water that influence the spectral properties depending on the concentration level (Figure 3.1 for montmorillonite; Lodhi et al. (1997)). Krachler et al. (2012) identified the phyllosilicates kaolinite, talc, and smektite, as well as carbonates calcite, magnesiumcalcite and protodolomite as the dominant drivers of salt pan turbidity, i.e. the amount of suspended materials (Jensen 2007), in Seewinkel. Montmorillonite cannot be found in Seewinkel salt pans, but is used here as it is the only phyllosilicate mixed with water that can be found in the USGS spectral library (Kokaly et al. 2017). It is also a member of the smektite mineral group that can be found in Seewinkel (Krachler et al. 2012). When abundant in water, it exerts a strong influence on the spectral properties between 0.38 μm and 0.9 μm as well as around 1.1 μm. Depending on the mineral content, similar spectral curves can be expected from inundated salt pans, as shown in Figure 3.1.

The spectral signature of the soil that sometimes surrounds the salt pans in question depends on the texture of the soil, the moisture content of the soil, the content of organic matter, the iron oxide content, the salinity of the soil and the surface roughness (Jensen 2007). Generally, the spectral curve of (dry) soil is characterized by moderate reflectivity in parts of the visible spectrum and by increasing reflectance towards the NIR domain ($\sim 1.0 \mu m$) (Jensen (2007);

Figure 3.1). Non-saline soil is similarly reflective as saline soil (Mougenot et al. 1993), but more reflective than water surfaces throughout the visible, NIR and SWIR spectrum (called middle infrared in Mougenot et al. (1993)). The reflectance of saline soils is strongly influenced by the moisture content and the spectral signatures of the observed minerals (Mougenot et al. 1993). Here, the SWIR spectrum can be used to quantify the moisture content (Mougenot et al. 1993). In Seewinkel, Csaplovics et al. (2018) identified the minerals halite, thermonatrite, trona, thenardit, burkeite, and hydroxilapatit as the most dominant in most salt pans, which can also be found on the ground of bare salt pans (Krachler 2007). Due to the similar spectral signatures between minerals abundant in the salt pans in Seewinkel and Stonewall Playa (US; Dickerson et al. (2014)), it is likely that the spectral signature of the salt pans in Seewinkel will roughly correspond to the spectral curve of Stonewall Playa (Figure 3.1). Playa evaporites in the form of polyhalite additionally indicate the possible spectral signature of the salt pans in Seewinkel (Figure 3.1).

The reflectance of vegetation is conditioned by the leaf pigments and the leaf water content (Jensen 2007). The photosynthetic activity is influenced by vegetation vitality and the amount of incident photosynthetically active radiation (PAR). The reflectance of PAR (that is roughly equivalent to visible light) is largely driven by chlorophyll absorption of red and blue light. In the NIR spectrum, the spongy mesophyll drives scattering, while the amount of leaf water is responsible for a decrease in reflectance in the NIR and SWIR domains (around 1.45 μm, 1.94 μm and 2.7 μm) (Jensen 2007; Gitelson et al. 1998). Hence, in the case of low leaf water content, the spectral curve after $\sim 1.2\mu m$ appears more flat (Gitelson et al. 1996). This is also visible for the spectral signature of rangelands in Figure 3.1. The vegetation around the salt pans in Seewinkel is mostly grass, reeds, bushes, and rarely trees (Zimmermann-Timm et al. 2021; Krachler 2007) and is therefore comparable to rangeland. In some cases, agriculture borders directly on the salt pans basins. Due to the observation period spanning April-October, seasonal changes in vegetation health and cover occur, especially in the case of farmland. This seasonality has been taken into account by training a separate model for each month (see Schauer et al. (2023)).

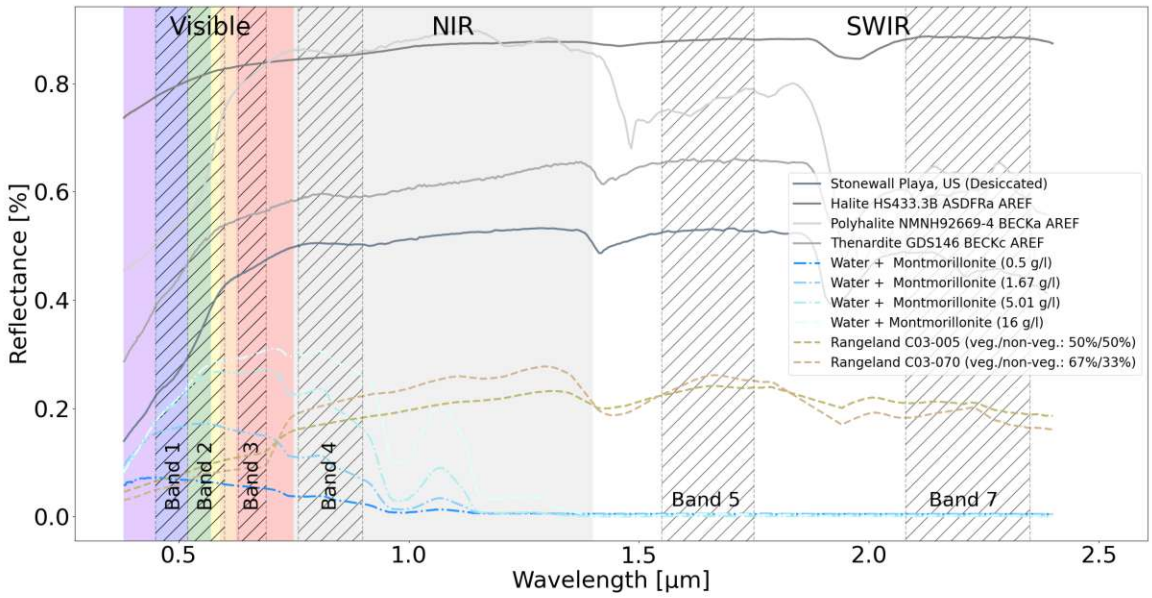

Fig. 3.1: Spectral properties of various types of solids, vegetation and liquids in the context of salt pans in the range of 0.38 μm to 2.4 μm based on the USGS spectral library (Kokaly et al. 2017). Spectral domains (visible, near-infrared (NIR), short-wave infrared (SWIR)) are additionally indicated together with the respective Landsat 4-5 Thematic Mapper (TM) bands (web address: `https://www.usgs.gov/landsat-missions/landsat-5` (accessed on 27 October 2023)).

Landsat bands for identifying water pixels and non-water pixels can be used separately (see Figure 3.1) or in combination. We utilized three indices that are suitable for identifying surface water: the normalized difference vegetation index (NDVI, Rouse et al. (1974)), the normalized difference water index (NDWI, McFeeters (1996)) and the modified normalized difference water index (MNDWI, H. Xu (2006)). NDVI is a widely used remote sensing technique used to assess and monitor vegetation abundance and health and has been shown to aid the successful identification of water bodies (Pekel et al. 2016). It quantifies the photosynthetic activity and density of vegetation cover by calculating the normalized difference between NIR and red light reflected by the Earth's surface via the formula:

$$NDVI = \frac{NIR - Red}{NIR + Red} \tag{3.2}$$

The NDVI can take on values between -1 (low photosynthetic activity) and 1 (high photosynthetic activity), depending on the strength of reflectance increase towards the NIR domain. The same concept is applied to water in the case of the NDWI (McFeeters 1996), although utilizing the strength of reflectance decrease towards NIR frequencies (Ji et al. 2009). The NDWI is designed to detect and quantify the presence of water in various landscapes. It is calculated using the ratio of the difference between green light and NIR radiation:

$$NDWI = \frac{Green - NIR}{Green + NIR} \tag{3.3}$$

NDWI has been shown to exhibit suboptimal performance in pixels characterized by the presence of urban built-up (Chiloane et al. 2020), as these surfaces exhibit a weaker NIR spectral response (H. Xu 2006). Therefore, the MNDWI utilizes the SWIR domain instead of the NIR domain to improve surface water detection. The spectral absorption of water throughout the SWIR domain is large and, more importantly, differs more strongly from the built-up areas compared to the NIR domain (H. Xu 2006; Jensen 2007). It is calculated using the ratio of green light to SWIR radiation:

$$MNDWI = \frac{Green - SWIR}{Green + SWIR} \tag{3.4}$$

Additional, more recent, indices have been developed, such as the Automated Water Extraction Index (Feyisa et al. 2014), the Water Ratio Index (L. Shen et al. 2010) and the Land Surface Water Index (Sakamoto et al. 2007). Still, the three indices presented above have proven to be performant indices and provide a stable basis for the classifcation task.

3.1.2 Problems of optical remote sensing for salt pan water extent

In the context of optical remote sensing for the analysis of the WE of salt pans, there are three primary problems that need to be addressed (Jensen 2007):

- Suspended material: as explained above, large amounts of suspended material in salt pan water bodies may impeed the clear discrimination between water and the surrounding soil in the visible and NIR spectrum (Figure 3.1). Especially the identification of turbid water in contrast to the minerals part of the desiccated salt pan soil has been proven to be problematic (Bowen et al. 2017).
- Illumination Conditions: optical remote sensing relies on solar radiation to capture images. The quality of the data is affected by factors such as the acquisition angle, which determines the angle at which the sensor observes the surface, and whether the data are collected during diurnal or nocturnal conditions (Schaepman-Strub et al. 2006). Different lighting conditions can impact the visibility and accuracy of salt pan WE information.
- Clouds: cloud cover in the atmosphere can obstruct the passage of light and affect the quality of optical remote sensing data (X. Li et al. 2021). Cloud cover can result in limited or obscured images, making it difficult to accurately assess salt pan WE (Ju et al. 2008), especially in areas with regular cloud cover such as Seewinkel during winter. Additionally, pixels affected by cloud shadowing should be treated to increase retrieval accuracy (Zhai et al. 2018; Shahtahmassebi et al. 2013; Amin et al. 2012).

Addressing these problems is crucial for ensuring the effectiveness of optical remote sensing techniques in monitoring and analyzing salt pan WE, as they directly impact data quality and the ability to make accurate assessments. Further details are described in Schauer et al. (2023).

3.1.3 Alternative remote sensing techniques of salt pans

Microwave remote sensing commonly encompasses frequencies from $1mm$ to $1m$ and can be divided into active systems (radars) and passive systems (radiometers) (Ulaby et al. 1981). Radiometers build on the radiation that is naturally emitted by the earth's surface and typically have a very coarse resolution of over $10km \times 10km$ (Le Vine et al. 2006). Thus, radiometers have not been used for small-scale lake and water body monitoring. Active microwave remote sensing has been frequently used to monitor wetlands, because radar systems have the ability to penetrate through clouds and acquire images independently of solar illumination (Schlaffer et al. 2022; Hess et al. 2003; Prigent et al. 2007; Reschke et al. 2012). Synthetic-aperture radar (SAR) sensors offer high-resolution imagery based on radiation that is highly sensitive to open water surfaces (Schlaffer et al. 2022). However, due to the susceptibility of SAR imagery to wind (Bartsch et al. 2012), which is a large factor in Seewinkel (Krachler et al. 2000), microwave frequencies were not used in the scope of this study. WH derived from radar altimeters is restricted to narrow tracks beneath satellite overpasses and, furthermore, too coarse for environments of small size (Birkett 2000; Schwatke et al. 2015). Additionally, understanding salt pan water variability can be done using WV. Data from satellite gravity missions (e.g. GRACE-FO; Kornfeld et al. (2019)) are too coarse to understand the salt pan WV in sizes down to 0.1 km^2.

3.1.4 Derivation of target variable

The methods to derive the target data (JASO inundation state) were provided by Stefan Schlaffer and are explained in detail in Schauer et al. (2023), Section 3.1.1.

3.1.5 Derivation of JASO inundation state

To derive the model target variable, an inundation state, that is 'desiccated' (0) or 'inundated' (1), was assigned to each year. This was completed based on the WE time series in JASO described above for nearly every year (1984–2022) and for each of the 34 salt pans individually. Due to the WE data gaps caused by cloud cover during the year 2002 (only acquisitions on 13 June 2002 and on 20 June 2002), this year could not be used for inundation state modeling. The only acquisition for the year 1999 in JASO, on 25 September 1999, did not result in WE data for Kiesgrube and St. Martins Therme 2 due to cloud masking. We decided to manually insert two states 'inundated' into the time series for the two salt pans after a visual inspection of the image, as otherwise the entire year would have been discarded. The year 2012 is missing in the inundation state time series due to the reasons described in Section 3.1.4.

In the case of a desiccation event, that is, a WE of zero, in any of the four JASO months for each year, the year was tagged as 'desiccated'. Correspondingly, in the event that no desiccation occurred, meaning a non-zero WE was present during the entire JASO period, the year was tagged as 'inundated'. Hence, a yearly and binary target space was formed. This resulted in a total of 1258 data points (37 years times 34 salt pans).

We decided to display the inundation state for each salt pan and year to increase the understanding of the model target. This was completed with the Python package matplotlib (Hunter 2007), as well as with all other data visualizations. Additionally, the month of the first desiccation event per year between April and October was visualized based on the original WE time series for spotting inundation events outside the JASO period. The first desiccation event per year is, furthermore, of key ecological importance (Krachler et al. 2012; Zimmermann-Timm et al. 2021).

3.2 Inundation state prediction

3.2.1 Exploratory data analysis: separability and correlation analysis

As a first step, we analyzed the feature space to unveil underlying distributions, feature relations, possible non-linearities in modeling, data complexity, and class separability (Morgenthaler 2009). This was completed by visual inspection of histograms per predictor and scatter plots between all predictor pairs in combination with class-based coloring using a seaborn pair plot (Waskom 2021). The complexity analysis was performed for two exemplary salt pans: Lange Lacke, which is one of the largest salt pans, and Unterer Stinkersee, which is known for its close connection to groundwater (Krachler et al. 2012). We abstained from a complete analysis for all salt pans via the maximum Fisher's discriminant ratio or other complexity metrics (Lorena et al. 2019) due to compactness and the ability of the RF to detect multi-dimensional patterns.

Furthermore, we performed a correlation analysis to gain an understanding of the temporal agreement between the predictive features. For this purpose, both Pearson's correlation coefficient r and Spearman's rank correlation coefficient ρ were calculated between the nine features with the scipy stats Python package (Virtanen et al. 2020).

3.2.2 Random forests

The RF approach was first proposed by Breiman (2001) and has since become a well-established algorithm in a number of scientific disciplines (Hastie et al. 2001). RF algorithms are commonly used in remote sensing (Belgiu et al. 2016; Dorigo et al. 2012) and are a widely applied method in practical data-driven hydrological research (Zounemat-Kermani et al. 2021; Tyralis et al. 2019). RF is built on ensembles of decision trees (Breiman 2001). The RF classifier can be expressed as the predicted value at the query point $m_{M,n}$ (Biau et al. 2016):

$$m_{M,n}(x;\Theta_1,...,\Theta_M,\mathcal{D}_n) = \begin{cases} 1 & \text{if} \frac{1}{M}\sum_{j=1}^{M} m_n(x;\Theta_j;\mathcal{D}_n) > \frac{1}{2} \\ 0 & \text{otherwise,} \end{cases} \tag{3.5}$$

where $m_{M,n}$ is a Borel measureable function[1], M is the number of trees, Θ_M are independent random variables used to resample the training set, x is a event of the random variable X, and

[1] A Borel measurable function is a function that preserves the measurability of sets. This concept is important in probability theory, integration theory, and various areas of analysis, as it allows to work with functions that behave congruently with respect to measurable sets and helps in defining integrals and handling probabilistic concepts (Trabs et al. 2021).

$\mathcal{D}_n$ is the original data set. In simpler terms, given X and D_n the model estimates a value of Y that is specified by the majority vote among the classification trees. The majority vote is estimated relative to the total number of trees M and results in class 1 given $m_{M,n} > \frac{1}{2}$.

The RF conceptual idea represents a twofold implementation of bagging, or bootstrap aggregation, more precisely both sample bagging (aimed at averaging) and feature bagging (aimed at tree decorrelation) (Breiman 2001) with the common goal of variance reduction. This focus turns out to be sensible, as sufficiently deeply grown decision trees naturally tend towards low bias (Hastie et al. 2001). The algorithm is expected to work well with small sample sizes (Biau et al. 2016; Ferreira 2022), despite limiting the functioning of both bootstrapping and decision tree subsampling. Furthermore, since RF is a sufficient algorithm, it uses all available data. Moreover, we assumed a strong relationship between the target pans (based on (Krachler et al. 2012)) which we exploited by using the scikit- learn (Pedregosa et al. 2011) multi-output option (web address: `https://scikit-learn.org/stable/modules/tree.html#tree-multioutput` (accessed on 14 August 2023)). This aims to improve generalization accuracy by estimating different salt pans in a simultaneous fashion within a single model (Faddoul et al. 2012). Its principal is that "(...) during traversal of the tree, every node is checked to determine whether a decision can be made for any of the currently undecided tasks (...)" (Linusson 2013; Faddoul et al. 2012). We applied extensive tools for model interpretability such as the calculation of the feature importance, e.g., by mean decrease in impurity (MDI, also gini index) or mean decrease in accuracy (MDA, also permutation importance) or partial dependencies (Friedman 2001; Goldstein et al. 2015) inside this study. The calculations here are based on the respective scikit-learn packages (Pedregosa et al. 2011). Among the predictors used in this study, all are time series exhibiting high cardinality. Hence, the use of feature importance based on MDI to comparison to ones based on permutation importance is justified (Breiman 2001; Altmann et al. 2010; Saarela et al. 2021). The RF approach is not susceptible to overfitting if hyperparameter tuning is applied (Probst et al. 2019).

3.2.3 Model setup

The inundation state in summer/fall serves as the target variable in our models. Using data until the end of March of each year, we predict whether a salt pan dries out ('desiccated') or remains 'inundated' during JASO of the same year. This binary classification scheme has already been used as the basis for modeling WE in a number of studies (Solvik et al. 2021; Shaeri Karimi et al. 2019; Riley et al. 2023). The simplicity of the inundation state in summer/fall, meaning its low temporal resolution, its low number of classes, and its low degree of mathematical abstraction (Section 3.1.5), in combination with our predictor setup and the RF algorithm, leads to relatively good model performance and model interpretability. The inundation state in summer/fall comprises a number of advantages: it is relatively robust considering the inhomogeneous number of acquisitions per year; it closes the lack of preceding research by introducing a classification task with a low number of classes; it addresses important hydrological and ecological issues, as many plants and animals in Seewinkel rely on water abundance within

the salt pans during summer/fall (Dvorak et al. 2016; Dvorak et al. 2020; Krachler et al. 2012); it is of interest to decision-makers that can use our models to enable efficient water management by, e.g., steering artificial inundation; and it further helps us to identify the most useful predictors quantifying refilling during winter/spring months, as it is aimed at the core characteristic of salt pans (Lowenstein et al. 1985), namely the yearly inundation state in JASO. The main limitations of the target chosen in this study are its coarse temporal resolution and the omittance of spring inundation/desiccation events that are of high ecological importance (Dvorak et al. 2020; Krachler et al. 2012).

Although the prediction is only made once per year, lead times vary between three and six months as the drying events accounted for by our model can happen in any month from July to October. Despite desiccation sometimes also occurring before July, we aimed for a setup that enables forecasting. This is, on the one hand, more challenging because we include longer lead times, but, on the other hand, more valuable for policymakers and stakeholders.

To gain a thorough understanding of the predictors of salt pan desiccation while ensuring global model transferability, we developed four RF models. The model GROUNDWATER only uses in situ groundwater information, the model METEOROLOGY uses only meteorological data, and the COMBINED model uses both groundwater and meteorological predictors (Table 2.1; sometimes referred to as main models). In addition, we developed the RANDOM model, based on a single predictor randomly sampled from a uniform distribution to create a baseline for testing model performance by involving chance.

For each of the four models, we followed the same training, validation, and test splitting (Joseph 2022; Y. Xu et al. 2018). We use the definition of Ripley (2007), who defines the validation set via the use of hyperparameter tuning and the test set via the use of a final and independent evaluation of the model. The model splits are presented in Figure 3.2. We followed an approximate overall 70% (training), 10% (validation), and 20% (testing) split. For hyperparameter tuning (described in Section 3.2.5), we applied a six-fold stratified cross-validation (CV) within the 80% model validation set that recurrently applied the approximate 70%/10% split. This roughly translates into an 85%/15% split relative to the entire model validation set (Figure 3.2).

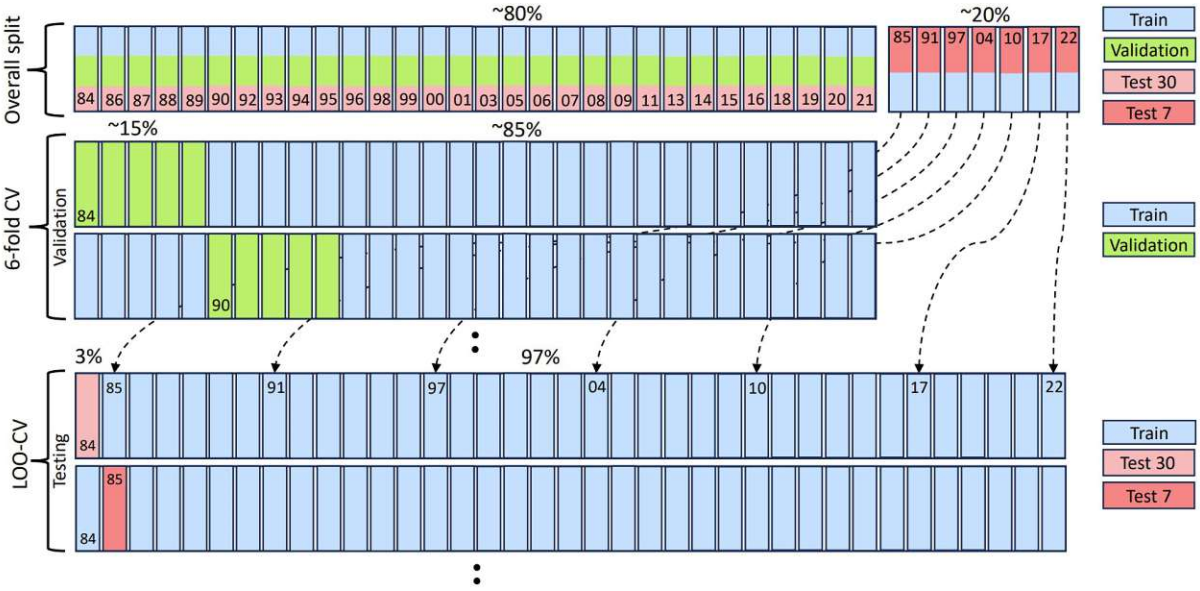

Fig. 3.2: Model splits separated into training sets (blue), validation sets (green), and test sets (pink). The years that correspond to each fold are indicated. Additionally, the cross-validation (CV) schemes are marked on the left side, and the arrows represent the introduction of the seven independent test folds to the leave-one-out cross-validation (LOOCV) scheme.

3.2.4 Model testing

Inside model testing (∼20% of the entire data set), we made use of a leave-one-out cross-validation (LOOCV) (Fukunaga et al. 1989; Wong 2015). This is meant to improve the prediction skill as always all other folds, except for the current single test fold, were used for model training as part of a recurrent 97%/3% split with respect to the entire data set (Figure 3.2). Hence, seven LOOCV runs were executed to test, each time, one year (at this point the independent year) of the overall seven independent test years. This independent test set (Test 7 in Figure 3.2) comprises the years 1985, 1991, 1997, 2004, 2010, 2017, and 2022. The years were chosen at roughly similar intervals across the entire temporal domain to ensure a balanced distribution of folds over time while maintaining the class balance of the entire data set.

While independent model testing uses ∼20% of the data (seven test years), we aimed to understand the year-wise model performance from 1984 to 2022. Hence, we reintroduced the folds used for model validation to model testing as part of a dependent test set. Here, the training data (∼80%, 30 additional years) were reused from model validation in the scope of the overall LOOCV (Test 30 in Figure 3.2). The year-wise information on metrics additionally benefits model understanding, as the target data exhibits skewed fold-wise class distributions that affect fold-wise model performance. Although the reintroduction enables the calculation of feature importance and partial dependencies for all folds, we abstained from such analysis due to small year-wise sample sizes. The reintroduction of the years used for model validation inherits the predisposition that these folds have been part of the hyperparameter tuning. Therefore,

the metrics for the folds of the dependent test set might be inflated as the hyperparameters were adjusted to exactly this set (model validation set).

As we did not want to exclude fold estimation for the initial training set, we used LOOCV instead of nested CV (Cerqueira et al. 2020), which is more commonly used for time series. The metrics for some salt pans may also be heightened due to a large target autocorrelation as we apply an LOOCV scheme (Cerqueira et al. 2020), although the effect is expected to be minimal due to the random characteristics (sample bagging) of the RF algorithm (Breiman 2001).

The estimations within the LOOCV scheme were carried out in the scope of 30 runs per main model. These repetitions aim to address the stochastic variability (randomness within the sampling and selection of features) of the RF approach (Breiman 2001). The results of the LOOCV were divided into training and test scores for the four model setups and two test sets (independent test set and dependent test set) and averaged over all runs. We calculated the standard deviation (SD) for model variability quantification but did not include it in the results, as it was generally low (max. SD of the Matthews correlation coefficient (MCC; Section 3.2.6) of 0.02 for the dependent test set (model GROUNDWATER); max. SD of the MCC of 0.03 for the independent test set (model RANDOM)).

For more insight, we calculated the average fold-wise LOOCV performance over all 30 model runs for the three main models (not the RANDOM model; Section 4.2.2). This provides information on the development of the test metrics over time. Additionally, random model realizations for the three main models were chosen to gain an in-depth understanding of model test set behavior (Section 4.2.3). This allows for studying the salt pan-wise inundation prediction, meaning the outcome as true positive (TP), false positive (FP), true negative (TN), and false negative (FN), for every year. The results for the RANDOM model were based on 200 repetitions to account for the random nature.

3.2.5 Model validation

For model validation, hyperparameter tuning was applied using *GridSearchCV* (Bergstra et al. 2012). The final hyperparameters used for the three models can be seen in Table 3.1. We used the hyperparameters from the COMBINED model for the calculation of the RANDOM model, as they offer the most robust solution against overfitting due to the larger number of features compared to the GROUNDWATER model and METEOROLOGY model.

Tab. 3.1: Hyperparameters chosen for the three model setups: GROUNDWATER, METEOROLOGY, and COMBINED. The numbers in parentheses relate to the average test set and training set performance given together with the standard deviation (SD; again, in parentheses). Furthermore, the entire selection of tested parameters, as well as the default parameters as proposed by scikit-learn (Pedregosa et al. 2011), are indicated.

Hyperparameter	**GROUNDWATER (0.6 (0.15)/0.65 (0.03))**	**METEOROLOGY (0.53 (0.12)/0.58 (0.02))**	**COMBINED (0.58 (0.14)/0.65 (0.03))**	**Tested Range by *GridSearchCV***	**Default**
n_estimators	40	40	40	40, 100, 300	100
max_feature	log2	log2	all	sqrt, log2, all	sqrt
max_depth	2	4	2	1, 2, 3, 4	ultd.
min_samples_leaf	5	3	7	3, 5, 7, 9, 10	1
min_samples_split	10	17	10	6, 10, 13, 17	2
max_leaf_nodes	5	2	7	2, 3, 5, 7	ultd.

Throughout the parameter-tuning process, *GridSearchCV* was performed with a six-fold stratified CV that uses an approx. 85%/15% split within the model validation set, as described in Section 3.2.4. Hence, for each validation run, five years were introduced as the actual validation set. The hyperparameter tuning was based on the definition of a range of values deemed sensible by the literature (Probst et al. 2019). Individual hyperparameters were varied within the predefined range and compared with performance differences of the training and validation sets. This gave a rough indication of and lever against overfitting. Subsequently, a further, more restricted range of hyperparameters was declared that allowed for training–test score differences of a maximum of 25%. Once more applying *GridSearchCV*, this range of values (Table 3.1) was tested using the MCC as the indicator. This resulted in the final set of hyperparameters also displayed in Table 3.1.

The hyperparameters were chosen using a different CV scheme and, hence, different model splits compared to the LOOCV scheme of the main models. The results obtained in the scope of the hyperparameter tuning were slightly worse compared to the test scores. In combination with the removal of the seven test folds, independent model testing is ensured, as hyperparameters adjusted to a certain split are prevented. The hyperparameters for all models (Table 3.1) are less complex compared to the default scikit-learn ones that are designed to fit a maximum of use cases (Buitinck et al. 2013). Generally, the decision trees have similar complexity between the models. The exact number of trees (40, 100, or 300) is not essential for model performance, as was verified both by varying the number of trees and by the CV results provided by *GridSearchCV*.

3.2.6 Evaluation metrics

Global confusion matrices with an MCC, F1-Score, and OA were calculated for the training sets, test sets (Test 7 and Test 30), and validation sets as the main indicators of the classification performance. Since we have a slight class imbalance, but both classes are equally important, we

performed macro-averaging to compute the F1-score to put equal weight on both classes (Opitz et al. 2019). As the F1-Score does not consider TNs, and the overall accuracy is vulnerable to a skewed class distribution (Chicco et al. 2020), the main metric considered in this study is the MCC. It is a robust metric regardless of class imbalances (Q. Zhu 2020). In the case of the main models, the metrics, in addition to being averaged over the 30 model runs (200 for the RANDOM model), were either averaged over all folds and salt pans based on the LOOCV scheme (Fukunaga et al. 1989; Wong 2015) or averaged over all salt pans for a single fold. To gain a salt pan-wise understanding of the model performance, the metrics were averaged across all years for the random model realizations described in Section 3.2.4 for the eight salt pans that exhibit a balanced class distribution. It was not possible to include the results for many of the salt pans due to the model's tendency to predict a single class in the case of a highly skewed class distribution per salt pan. We applied the formulation of the MCC used in scikit-learn (Pedregosa et al. 2011):

$$\text{MCC} = \frac{TN \times TP - FN \times FP}{\sqrt{(TP + FP)(TP + FN)(TN + FP)(TN + FN)}} \tag{3.6}$$

3.2.7 Feature importance

For model interpretability, we calculated the feature importance by the mean decrease in impurity (MDI, also Gini index) (Rebala et al. 2019) and partial dependencies (Friedman 2001; Goldstein et al. 2015). The results for the MDI were averaged separately for each of the three main models over all CV folds and model runs. Since the predictors used in this study are all time series that exhibit high cardinality, the use of feature importance based on the MDI is justified (Breiman 2001; Altmann et al. 2010; Saarela et al. 2021). Partial dependency plots (PDP) and individual conditional expectation (ICE) plots (Friedman 2001; Goldstein et al. 2015) were calculated for each salt pan individually using the training set for the test fold 1984, as this includes the most recent information. We interpret the PDP or ICE curve as the probability of predicting 'inundated' or 'desiccated' given different predictor values, as can be performed for a binary classification (Molnar 2020). The PDP and ICE plots were based on the COMBINED model's run, which is also displayed in Section 4.2.3. Salt pans with an especially large partial dependency, spread with regard for the respective predictor, were manually chosen and visualized, in addition to the PDP, by the ICE plots (Goldstein et al. 2015). The spread was calculated by subtracting the minimum partial dependence value from the maximum partial dependence value for each salt pan and predictor combination. For Heidlacke, Hottergrube, and Gsigsee, no partial dependencies could be calculated as only the state 'desiccated' is present. Both algorithms are based on the respective scikit-learn packages (Pedregosa et al. 2011).

4. Results

4.1 Salt pan mapping

The results of the models used for the retrieval of WE were provided by Stefan Schlaffer and are described in section 4.1 in Schauer et al. (2023).

A total of 60% of the complete inundation state data set (754 combinations of years and salt pans) are classified as 'desiccated', and 40% (504 events) are classified as 'inundated' (Figure 4.1a). For individual salt pans, the class distribution is highly heterogeneous, with a class imbalance of up to 100% in the case of Hottergrube, Heidlacke, and Gsigsee. For some salt pans, e.g., Lange Lacke, Unterer Stinkersee, or Herrnsee, extensive years of drought are needed to force drying. Unterer Stinkersee (type: 'naturally perennial') falls dry less frequently compared to Lange Lacke (type: 'periodically filled'). Salt pans that regularly fall dry are, e.g., Hochstätten, Fuchslochlacke 1 and 2, Huldenlacke, or Oberer Stinkersee. For Darscholacke, Zicksee, Kiesgrube, and Badesee Apetlon (type: 'artificially perennial'), an inundated state can be observed for nearly all years. Numerous salt pans fell dry six years in a row from 2016 to 2022, the longest (nearly common) desiccation period since 1984. In many cases, the year-wise distribution is similarly skewed as in recent years. The 'inundated' state commonly occurs clustered in time and over multiple pans. For example, the three periods in (and around) the years 1987, 1997, 2010, and 2015 are dominated by the state 'inundated', while around the years 1984, 1992, 2003, and 2007, and all years since 2016, the class 'desiccated' prevails.

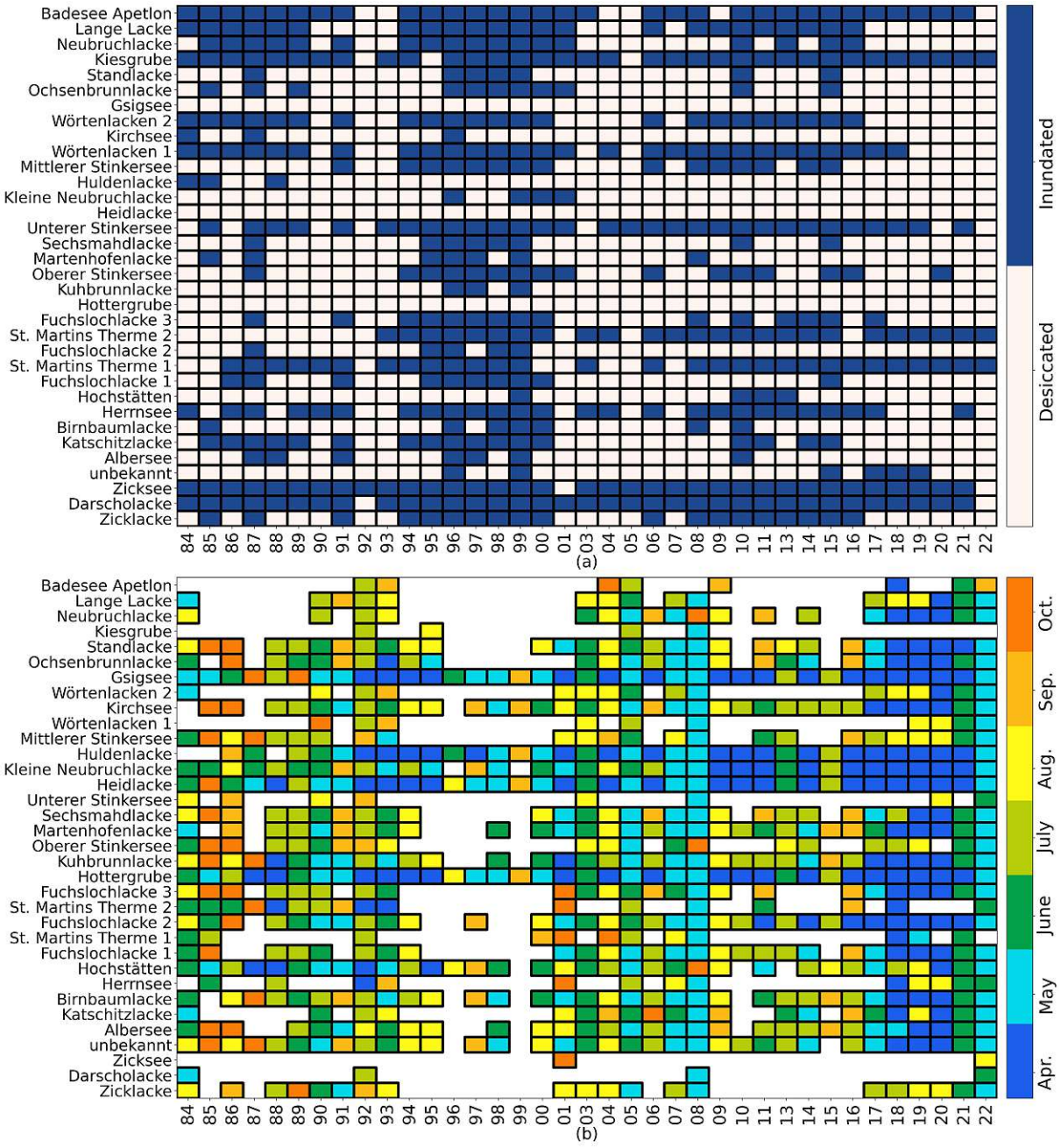

Fig. 4.1: (**a**) Binary classification into 'desiccated' state (light grey) and 'inundated' state (dark blue) for each salt pan and for each year. The years 2002 and 2012 are missing due to data gaps. (**b**) First month of each year in which the salt pans desiccate. Only months between April and October are shown.

As Figure 4.1b shows, in some years, (early) desiccation is prevalent; for others, inundation is present throughout the year (assuming the presence of water in winter). Since 2016, desiccation occurs earlier in the year compared to earlier periods. A total of 41 desiccation events outside the JASO period can be found when the 'inundated' state is prevalent.

4.2 Inundation state prediction

4.2.1 Exploratory data analysis

We detected no trend over the study period for five features (GW Anom., GW lvl. ratio, SGI, P Anom., and SPI 6) and an increasing trend for the other four features (T Anom., Number of days above 25 ° C, E Anom., and SPI 24). As expected, the features that are connected to an increase in WE, e.g., groundwater and precipitation anomalies, have positive correlations with each other (Figure 4.2). The same applies to the features that are assumed to be connected to a decrease in WE, i.e., temperature, evaporation, and number of days above 25 ° C. Consequently, correlations between predictors associated with water gain and water loss, respectively, are negative. The relationships between features that build on integration periods other than 12 months (e.g., SPI 6) are less clear.

The histograms in Figure 4.2 suggest a better separability between the desiccation and inundation states for Lange Lacke (a) compared to Unterer Stinkersee (b). This is indeed confirmed by the inundation state classes in the scatter plots, which show more distinct clusters in the case of Lange Lacke. The plots suggest that groundwater-based features, especially SGI, are the most promising predictors for desiccation forecasting. They also reveal that no two-dimensional predictor combination can lead to perfect class separability on its own and that multiple features should be included in the models.

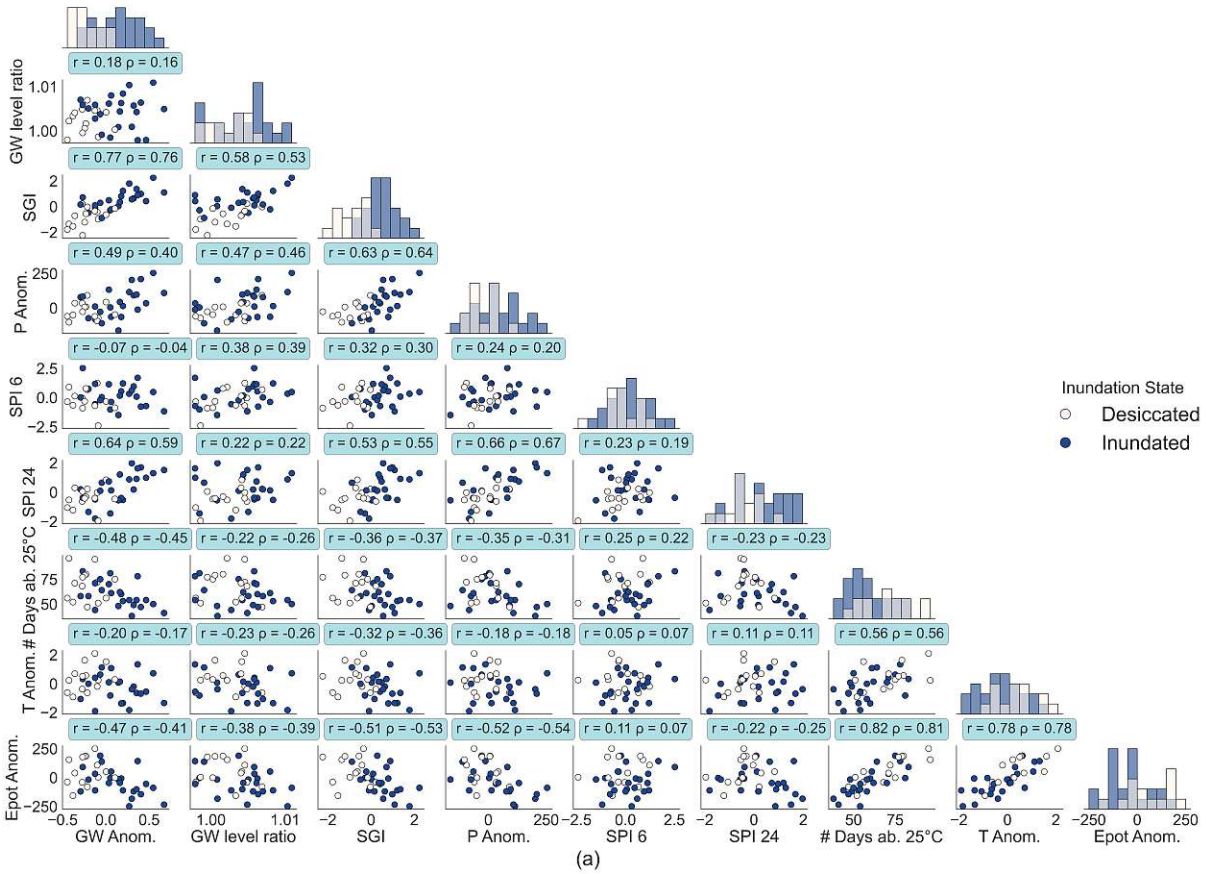

Fig. 4.2: *Cont.*

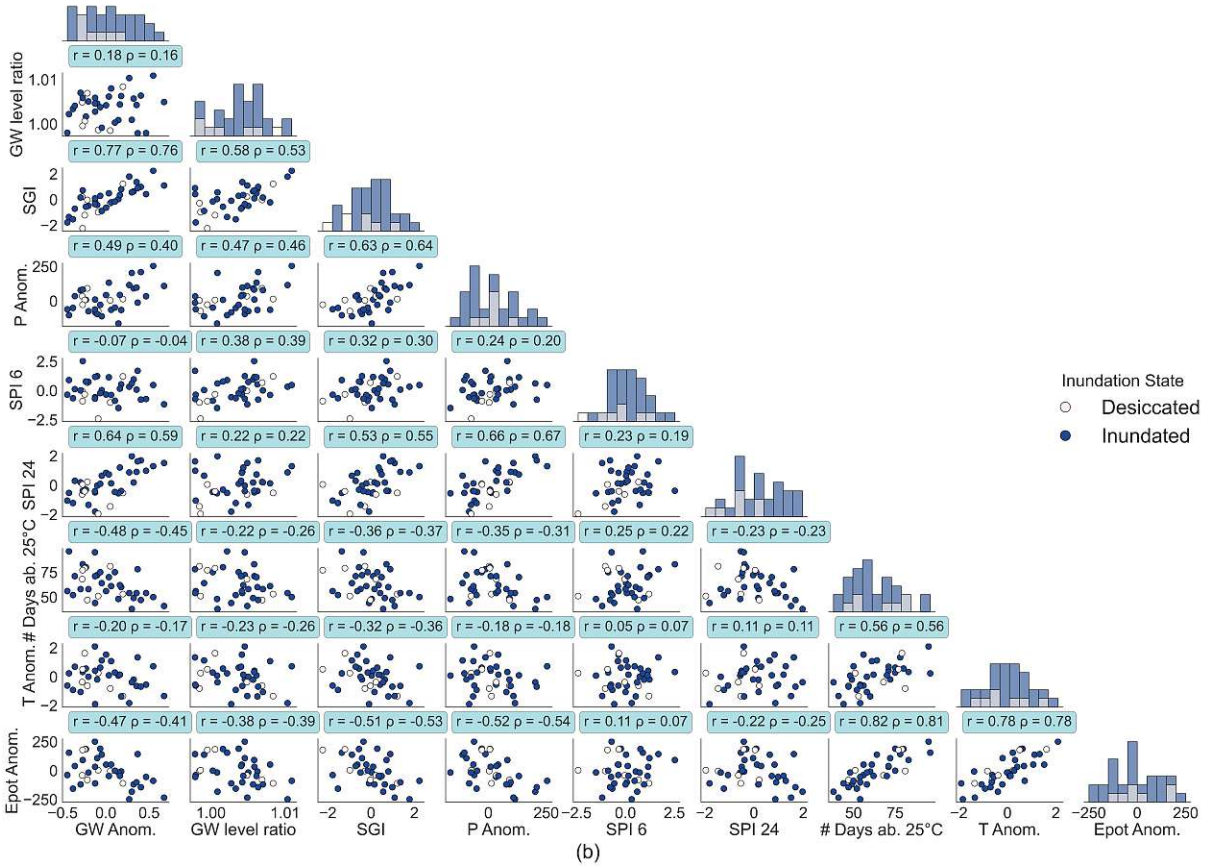

Fig. 4.2: Histograms and scatterplots for Lange Lacke (**a**) and Unterer Stinkersee (**b**) for all nine predictors with coloring in the respective classes. Correlation coefficients (Pearson's r and Spearman's ρ) are additionally displayed on blue background.

4.2.2 Average prediction skill

On average over all 37 folds provided by the LOOCV and 30 model runs, the three models have moderate skill with an MCC of approximately 0.6 (GROUNDWATER: 0.6, METEOROLOGY: 0.59, COMBINED: 0.6). For the independent test sets (seven test folds), a 0.24 performance increase with respect to the RANDOM model is obtained on average for the three models. Generally, the test metrics as averaged over all folds (described above) and the dependent folds (Table 4.1) confirm the abilities of GROUNDWATER in modeling the inundation state. The independent test set performance metrics of METEOROLOGY exceed those of GROUNDWATER. The COMBINED model does not show any increase in performance with respect to METEOROLOGY or GROUNDWATER. Averaged over all independent test folds and 30 model runs together, the MCC of METEOROLOGY is 0.09 (0.07) higher than that of COMBINED (GROUNDWATER).

Differences between the confusion matrices, as averaged over 30 model runs, are minimal between the three models (below 1% in regard to the entire sample; Figure 4.3). All three models struggle more with the correct estimation of state 'inundated' compared to 'desiccated'

(relation of FPs and FNs to the total number of state 'inundated' and 'desiccated', respectively). GROUNDWATER exhibits more skill in the classification of TNs (a surplus of nine TNs) compared to the METEOROLOGY model. COMBINED manages to achieve a surplus of one TP and nine TNs compared to METEOROLOGY. As discussed in Section 4.2.1, large salt pan inundation state variability results in extensive year-wise heterogeneity in the class distribution and model performance. As indicated by Figure 4.3, the performance between the folds is heterogeneous. The models perform better, and with less variability in terms of the MCC, for the independent test folds (GW 7, METEO 7, and COM 7) compared to the 30 dependent test folds (GW 30, METEO 30, and COM 30). Outliers excluded, the tested folds exhibit a pronounced dynamic over the years. Beginning in 2004, the estimates tend to improve. Here, the MCC does not fall below 0.5, neither for the seven test folds nor for the additional 30 test folds. In the years 2006 and 2007, the GROUNDWATER model performed much better for the 30 dependent test folds compared to the other two models. A very different picture is observed pre-2004: all three models struggle to achieve scores from above 0.5 to 0.6. Especially 1992 presents itself as challenging for the RF models.

All GW 7, METEO 7, and COM 7 (Figure 4.3) perform better compared to GW 30, METEO 30, and COM 30. With this in mind, the difference in metrics between the two sets, as displayed in Table 4.1 can be integrated more clearly.

Tab. 4.1: Average performance of different model setups inside LOOCV scheme separated for testing the seven independent test folds (1985, 1991, 1997, 2004, 2010, 2017, and 2022), and the thirty dependent test folds that have already been part of the validation set. Results are averaged over 30 model runs. As the SD was, in all cases, below 0.03, we disregarded this information for each metric.

Model/Score	**GROUND-WATER 7**	**METE-OROLOGY 7**	**COMB-INED 7**	**RAN-DOM 7**	**GROUND-WATER 30**	**METE-OROLOGY 30**	**COMB-INED 30**
MCC-Test	0.59	0.66	0.57	0.36	0.61	0.57	0.61
MCC-Train	0.68	0.66	0.68	0.56	0.68	0.66	0.68
F1-Macro Test	0.79	0.83	0.78	0.68	0.80	0.79	0.81
F1-Macro Train	0.84	0.83	0.84	0.78	0.84	0.83	0.84
Accuracy Test	0.80	0.83	0.79	0.7	0.81	0.80	0.82
Accuracy Train	0.85	0.83	0.85	0.79	0.85	0.84	0.85

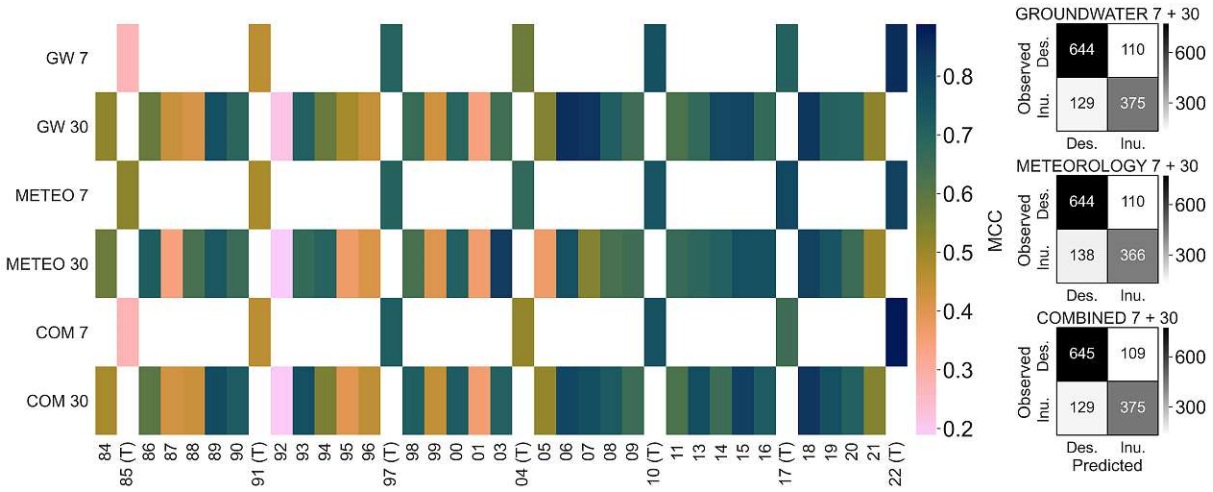

Fig. 4.3: Fold-wise average Matthews correlation coefficient (MCC) over 30 model run for every model (GW—GROUNDWATER, METEO—METEOROLOGY, COM—COMBINED) and split. The averaged confusion matrices over 30 models run for all 37 folds are additionally displayed for all three models. The folds from independent test set are marked with (T).

4.2.3 Detailed analysis of single LOOCV model runs

All three models successfully predict the diverse interannual dynamics of the inundation state per salt pan (Figure 4.4). TPs and TNs are numerous, especially in the years with average conditions. Overall, an accurate estimation in times of pronounced dry and especially wet periods appears more challenging. For instance, the models lack adequate prediction for the dry periods in 1986, 1992, 2003, 2007, 2011, and 2016, as well as for the wet periods in 1987 and around 1996 (1997), 2010, and 2015.

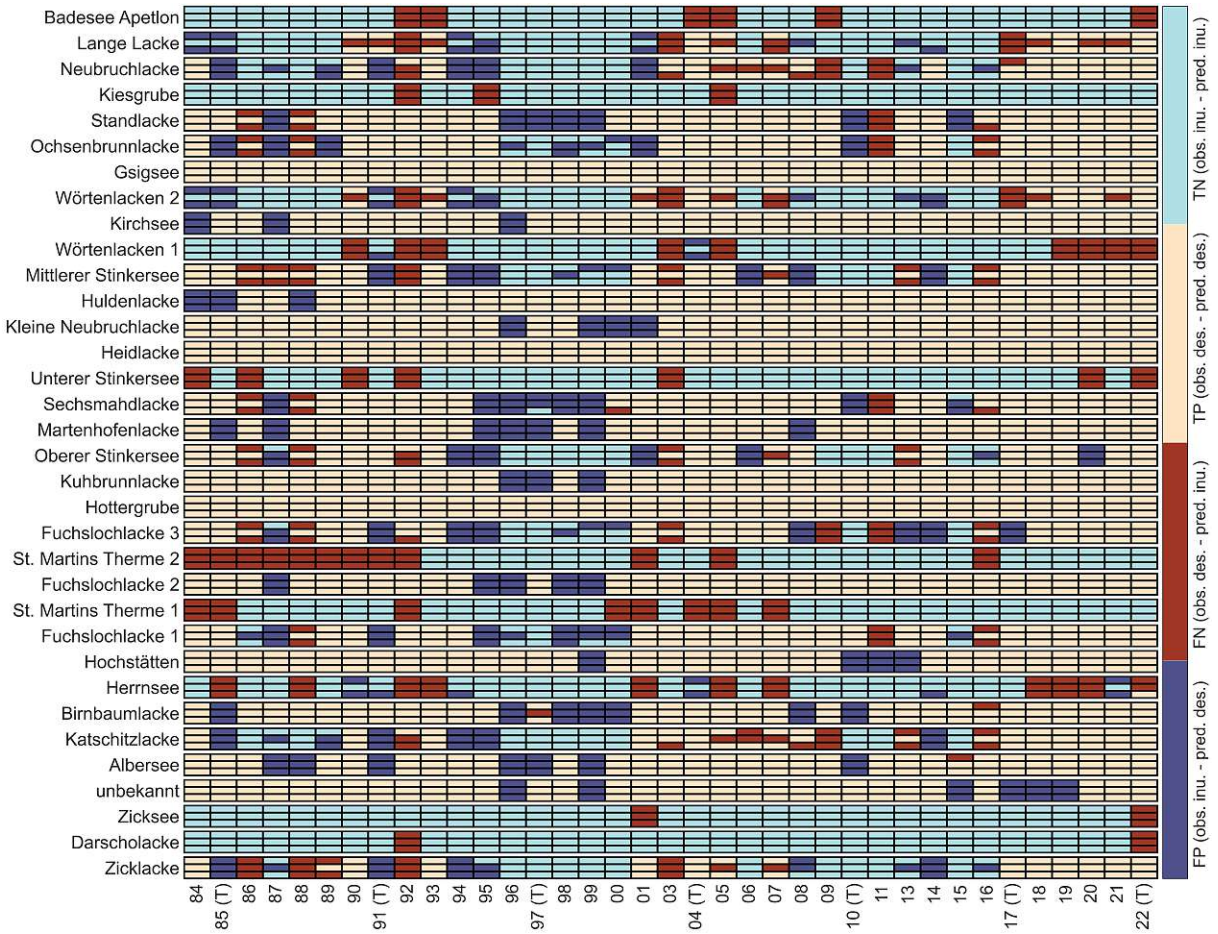

Fig. 4.4: Confusion matrix outcomes for all years (part of this study) from 1984 to 2022 for the three main models based on the results for the dependent and independent test sets. For each salt pan (3 rows), the top-most row represents the GROUNDWATER model, the middle row represents the METEOROLOGY model, and the last row represents the COMBINED model. The underlying confusion matrix is rolled out for all 34 salt pans as a function of time. Again, the folds from the independent test set are marked with (T).

For 18 salt pans with a dominant state, the events are correctly predicted in favor of the majority class (a co-occurrence of light blue and dark red and of light red and dark blue, respectively, in Figure 4.4). In these cases, the estimates between the three main models (i.e., GROUNDWATER, METEOROLOGY, and COMBINED) do not differ, e.g., Badesee Apetlon. Differences between the models exist for 16 salt pans but are only marginal for Standlacke, Ochsenbrunnlacke, Wörtenlacken 1, Sechsmahdlacke, Fuchslochlacke 1, Herrnsee, Birnbaumlacke, and Albersee. The eight cases with varying results between the models are Zicklacke, Katschitzlacke, Fuchslochlacke 3, Oberer Stinkersee, Mittlerer Stinkersee, Wörtenlacken 2, Neubruchlacke, and Lange Lacke. These salt pans feature a more balanced underlying class distribution with varying class succession. Here, the models demonstrate their flexibility, i.e., the ability to estimate different states for subsequent years. When there is a shift from periods

of 'inundated' to 'desiccated', or vice-versa, the models do not correctly predict wet and dry states for many salt pans. For instance, correct estimates for wet conditions in 1994 and for dry conditions in 2016 emerge one year later after a dry period (around 1993) or wet period (around 2015) (Figure 4.4). The strength of model GROUNDWATER lies in its ability to more precisely identify wet, and, in particular, dry episodes compared to model METEOROLOGY (the identification can be salt pan-specific). Examples here include Lange Lacke and Wörtenlacken 2 around 1991 and Neubruchlacke, Katschitzlacke, and Zicklacke after 2004. The METEOROLOGY model struggles to achieve this, often failing to correctly estimate for a number of years in a row (e.g., Neubruchlacke around 2006 and Zicklacke around 2014). However, for many salt pans, the model performed better in 1986 and 1988. In a number of additional instances, the METEOROLOGY model manages to outperform the other two. This translates into the correct estimation of single anomalous events before and after extremely wet or dry conditions. Examples include Ochsenbrunnlacke, Mittlerer Stinkersee, Fuchslochlacke 1, Fuchslochlacke 3, and Katschitzlacke in 2016 (as outcome TP) or Lange Lacke and Wörtenlacken 2 in 1994 (as outcome TN). The COMBINED model performs similarly to the GROUNDWATER model, though it surpasses its performance in a few cases (e.g., Mittlerer Stinkersee in 1999 and 2000). In these cases, the model is able to integrate meteorological and groundwater-based information in a productive manner.

The MCCs for the eight salt pans that exhibit a more balanced class distribution differ between the three models and between the salt pans (Table 4.2. On average, the GROUNDWATER model performs best with a moderate MCC of 0.44 and the METEOROLOGY model performs the worst (0.29). The COMBINED model attains an MCC of 0.37. For Fuchslochlacke 3 and Mittlerer Stinkersee, the METEOROLOGY model performs better than the GROUNDWATER and COMBINED models, whereas the opposite is true for the other six salt pans. Compared to the overall model performance of 0.6, the models perform worse for these eight salt pans with an average MCC of 0.37.

Tab. 4.2: Salt pan-wise MCC (as averaged over all folds) for the three single model realizations (GW–GROUNDWATER, METEO–METEOROLOGY, COM–COMBINED) displayed in Figure 4.4 for the eight salt pans that exhibit a balanced class distribution.

Average MCC	Zicklacke	Katschitz-Lacke	Fuchsloch-Lacke 3	Oberer Stinkersee	Mittlerer Stinkersee	Wörten-Lacken 2	Neubruch-Lacke	Lange Lacke	Mean
Model GW	0.46	0.51	0.13	0.5	0.15	0.6	0.57	0.6	0.44
Model METEO	0.2	0.34	0.37	0.51	0.49	0.13	0.19	0.11	0.29
Model COM	0.46	0.35	0.15	0.4	0.28	0.44	0.4	0.44	0.37

4.2.4 Feature importance

In the GROUNDWATER model, GW anomalies and the SGI have comparable importance (around 0.35, respectively) while this is lower for the GW level ratio (Figure 4.5). In the METEOROLOGY

model, SPI 6 has little importance while the predictors derived from temperature have highest importance. SPI 24, although substantially correlated with GW anomalies and the SGI ($r = 0.64, r = 0.53$, respectively; Section 4.2.1), which are important in the GROUNDWATER model, has a lower importance than the temperature predictors. These observations are in contrast with COMBINED, where the SGI has the highest importance by far. With a mean importance of 0.47, it is much larger than the other predictors, most of which lie at a maximum of ∼0.05. Only groundwater and temperature anomalies have an importance >∼0.05.

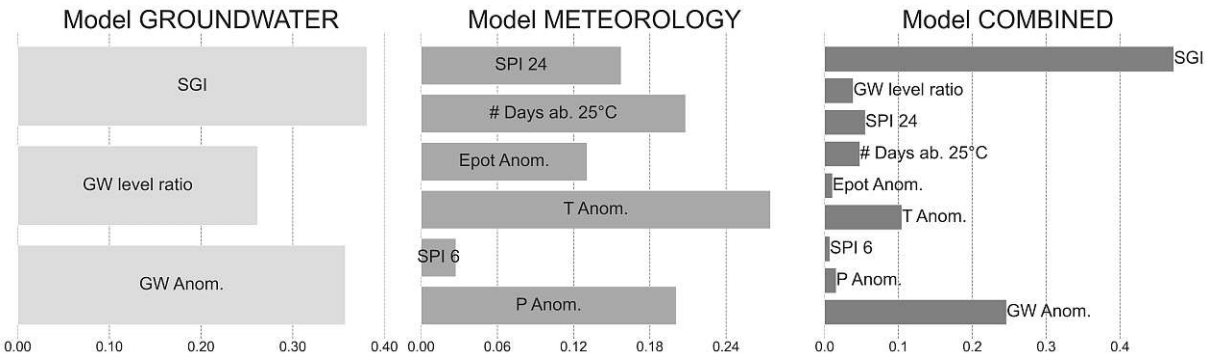

Fig. 4.5: Feature importance calculated as average across all folds and 30 model runs for the three main models.

4.2.5 Partial dependency

The potential significance of groundwater-based predictors to estimate the inundation state of Lange Lacke (Section 4.2.1) translates into a pronounced evolution of partial dependency against the SGI (Figure 4.6, steel-gray dashed) in the COMBINED model (also for Wörtenlacken 2). SPI 24 has a comparable impact on Unterer Stinkersee (light blue dash-dotted), although to a lesser extent. It is striking that the other predictors do not, or only slightly, affect the prediction skills in both cases. Statistically, when involving the entire population of 34 salt pans, the variability in the inundation states of nine salt pans can be explained mainly by meteorological predictors, whereas, in 22 cases, groundwater-based features perform best (Table A.1, Appendix A). In some cases, there is only little variability of the partial dependency when plotted against any of the predictors. This is also indicated by Table A.1, though it is not further regarded here due to compactness. We find that, except for the E_{pot} and SPI 6, every predictor exhibits a strong interaction with the dynamics of at least one salt pan (Table A.1; Figure 4.6 in dotted red). Groundwater-based features exhibit more pronounced curves that span a wider partial dependency range compared to the other predictors.

In general, the partial dependencies agree with the underlying physical process. For instance, higher temperature anomalies (Kirchsee) or the number of days above 25 °C (Katschitzlacke) contribute to a prediction probability in favor of the 'desiccated' inundation state. This rule is not true for all salt pans, although this dependence commonly applies. The PDP reveals all important probability thresholds for inundation state prediction. For example, at $SGI = 0$, the class attribution probability switches from the 'desiccated' state to the 'inundated' state for

Lange Lacke. At around 60 days above 25 °C in the previous 12 months, the estimates change from 'inundated' to 'desiccated' for Katschitzlacke. Similar inferences for nearly all salt pans can be made. These are summarized in Appendix A.

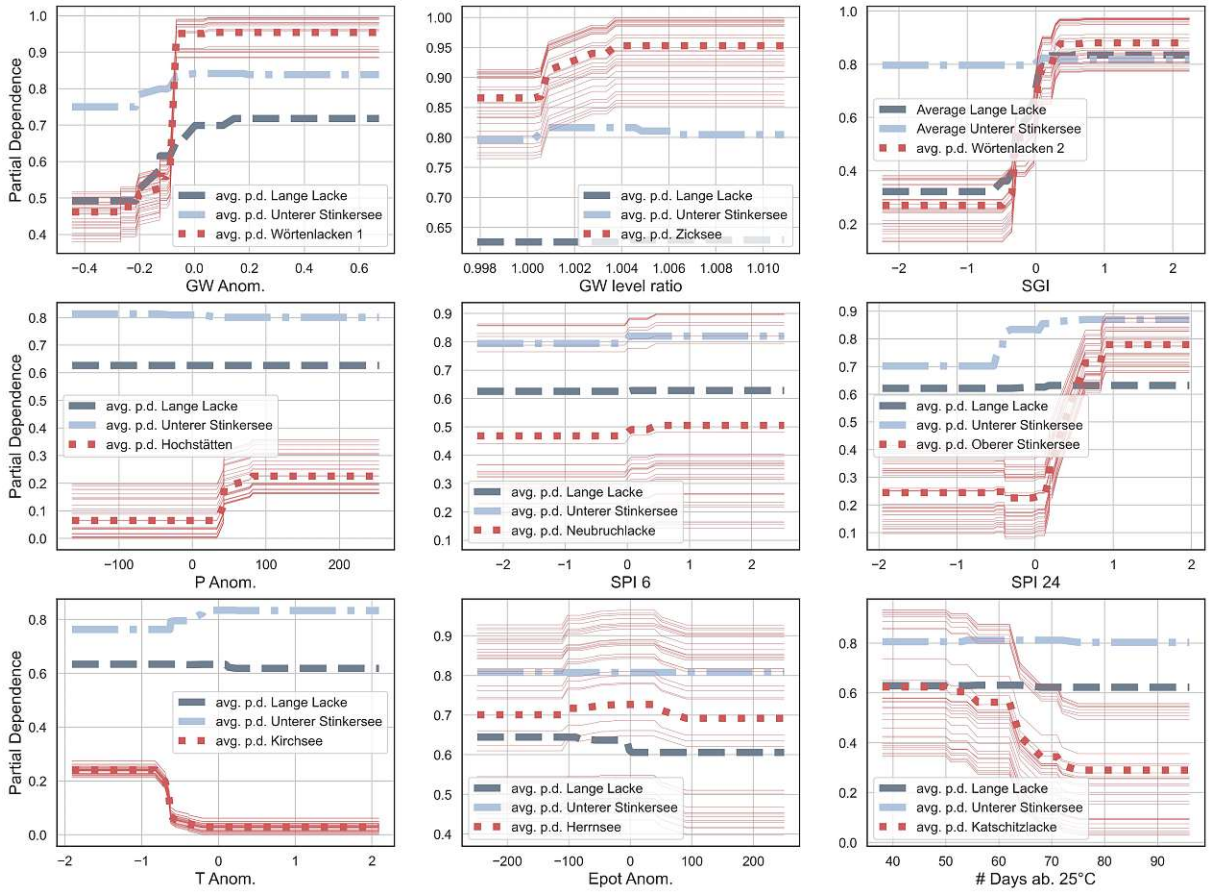

Fig. 4.6: The Partial Dependency Plots (PDP) are displayed for each predictor inside the COMBINED model for three selected salt pans: Lange Lacke, Unterer Stinkersee, and, additionally, a salt pan with a pronounced partial dependency dynamic against the respective predictor. For these salt pans, the individual conditional expectation (ICE) plots are also included in red with reduced line width.

5. Discussion

5.1 Assumptions

The modeling framework has been built on several assumptions. First, the targets (i.e., inundation dynamics for different salt pans) are correlated. Second, the accumulation periods (particularly, the dominant 12-month period) hold explanatory power in regard to the inundation state in summer. Third, the salt pans are in an environmental condition that is good enough to allow them to react to the natural drivers applied in this study. In other words, the salt pans need to be at least sufficiently well connected to the salt pan cycle to respond to the groundwater-based and meteorological predictors. Fourth, we assume that the climatology always leads to the prediction of a drying from spring toward summer. Hence, the models cannot predict the 'inundated' state based on dry conditions in spring. This is unless the salt pan-wise class distribution is skewed towards the 'inundated' state, causing the models to always predict the 'inundated' state (outcome TN). In other words, if the situation during the lead time deviates much from the climatology, the models will not capture many of the effects on the salt pan inundation state. This is a disadvantage in years when drivers strongly change and may lead to misclassifications.

In total, desiccation in spring (in April to June; here used as a proxy for dry conditions) in combination with the 'inundated' state in JASO occurred for 41 events (Figure 4.1a) and resulted in 20 TNs and 21 FPs for the GROUNDWATER model. The year 2008 accumulated a notable number of fourteen FP outcomes. This circumstance also reveals that not all annual desiccation events were captured. Taking into account the desiccation events from the beginning of April to the end of October would result in a class distribution of 63%/ 37%.

5.2 Predictors

The results of the EDA (only for Lange Lacke; Figure 4.2a), feature importance (Figure 4.5), and calculation of partial dependencies (Figure 4.6) support the assumption of a close connection between salt pans and groundwater (Krachler et al. 2012; Zimmermann-Timm et al. 2021). We suspect that the rather long time steps of the model and the respective long-term predictor setup support the forcing of the slow-reacting features evolving around groundwater as a key predictor. It is to be determined whether the high importance of groundwater is actually due to the contribution of groundwater to salt pan water status directly or more generally to water abundance, i.e., drought conditions, in the region. The outstandingly high feature importance

of SGI is presumptively connected to its continuous nature, rather than relying on artificially thresholded integration periods (Bloomfield et al. 2013).

Still, the METEOROLOGY model achieved similar scores compared to the GROUNDWATER model. Both were able to capture many of the interannual differences in the inundation state. We managed to find meteorological predictors that are of importance for spring salt pan water abundance, which is essential for the salt pan inundation state in JASO. The importance of meteorological predictors could stem from their temporal autocorrelation from one year to the next (Sun et al. 2018; Cancelliere et al. 2010). For the meteorological predictors, a single (or more) not included month(s) from the previous year could make a change in spring water abundance.

We find that, other than the continuous SGI, time periods of 12 months or more work best for predicting salt pan inundation state. Such predictors exhibited large feature importance within their model setups. It is up to further research to determine whether the 12-monthly anomaly mean is the most appropriate integration period. This argument is particularly relevant as shifting climate patterns influence groundwater recharge. The SPI 6 and the GW level ratio relate to a similar time period (6 months). This period does not seem to be particularly relevant, as both predictors were comparatively insignificant in all three models (also when disregarding the SGI). Temperature-based predictors were most important in the METEOROLOGY model despite exhibiting low correlations with the SGI.

For some combinations of salt pans and predictors, the PDP (Figure 4.6) exhibited sigmoid curves with a wide spread. The PDPs for Lange Lacke and Unterer Stinkersee showed a clear progression against the SGI and SPI 24, respectively. The SPI 24 is closely related to groundwater drought as suggested in the literature (McKee et al. 1993) and by the correlation analysis ($r_{SPI24,SGI} = 0.53$ and $\rho_{SPI24,SGI} = 0.55$; Section 4.2.1). Therefore, our results can confirm the observation made by Krachler et al. (2012) that both salt pans are closely connected to groundwater. This is even more true for Wörtenlacken 2, which is reported to have an atypically strong connection to groundwater, even greater than that of Lange Lacke (Krachler et al. 2012). Similar inferences can be made for all other salt pans (Appendix A). Additionally, the probability thresholds for the SGI were similar in the case of Lange Lacke and Wörtenlacken 2 (Figure 4.6). However, such an analysis is prone to misinterpretations as partial dependency behavior can vary depending on the model setup and the underlying training data. For example, the hydrology of Katschitzlacke is reportedly similar to Lange Lacke (Krachler et al. 2012), whereas our results indicate a closer connection to the predictor number of days above 25 °C.

A drawback associated with the input data is their low spatial resolution. The argument is particularly valid for P anomalies, since groundwater level, E_{pot} anomalies, and T anomalies vary less in space and time (Tallaksen et al. 2009; Miralles et al. 2011). Here, future models could improve the (spatial) representation of precipitation. An understanding of the inundation state in JASO would require seasonal forecasts of hydrological and meteorological variables. Meteorological predictors that focus on depicting changing precipitation, evaporation, and temperature patterns in the region due to climate change should additionally prove beneficial (M. K. Vanderhoof et al. 2018).

Features evolving due to the human impact on the ecosystem, such as the (e.g., monthly) amount of groundwater extraction from wells and discharge into drainage canals, were not used, as, to our knowledge, no such information is available in the region. However, the use of this information could potentially enhance the knowledge to be gained from the models, especially if such information was available at the subregional scale or for each salt pan.

5.3 Target

Our results confirm that the EO-based inundation state is a useful target variable for ML-based modeling. Data from the Landsat mission has been shown to form a useful basis for quantifying interannual dynamics in surface water dynamics (M. Vanderhoof et al. 2016; G. Liu et al. 2011; Pekel et al. 2016). Although in some years, the impact of cloud cover was high, the summer/fall inundation status could be retrieved for all salt pans over the entire study period except for the years 2002 and 2012. The variation in this target variable roughly showed similar dynamics to some of the variables considered in other studies on a larger area, e.g., SPEI3 (Crocetti et al. 2020) or long-term precipitation (Hackl et al. 2023). The year 2015 represents an exception, as it is referred to as drought year in Crocetti et al. (2020) but appears rather wet in our analysis. This might be because of the rather wet conditions in fall-winter 2014, which is also visible in Crocetti et al. (2020).

Uncertainties in the salt pan time series are expected to be larger for smaller salt pans, which have a larger relative proportion of mixed pixels with bordering land (Section 4.1). However, this argument turns out to be secondary since the accuracy of the model target is dependent on the exact recognition of desiccation and not on the precise sensing of the true WE. Higher resolution remote sensing products, such as Sentinel-2 imagery, could reduce the error connected to spotting desiccation inside the 'last' pixels. Such data would need to be used in combination with, e.g., the Landsat archive, to build the models on extensive time series. In addition to using satellite data with higher resolutions, we propose the use of alternative target variables to avoid the skewed salt pan-wise (and year-wise) class imbalances. The time of the first desiccation (Figure 4.1) would constitute an interesting target variable (Krachler et al. 2012; Zimmermann-Timm et al. 2021).

5.4 Model error

Although in this study we were able to predict the salt pan inundation state in Seewinkel with only moderate accuracy, the average performance of the three independent test sets indicates a gain of 0.24 compared to the RANDOM model. We regard the average score between the models of 0.6 as acceptable only insofar as the assumed reasons for the observed model error are numerous and, depending on the salt pan and year, heavy-weighing. Therefore, the model error can be, approximately, explained. Increasing the model performance based on the issues described, in detail, below is largely limited by data uncertainty and data availability. The failure

of the model to make correct predictions if the meteorological conditions deviate much from the climatology, the artificial inundation, and the uncertain hydrological condition, meaning surface water possibly infiltrating into deeper layers, explain the results and provide starting points for future improvements to the model. In general, we consider the model setup performant and stable.

Many years exhibit highly skewed class distributions, especially since 2016. This influences the metrics since different years are connected to varying degrees of difficulty in correct estimation. The total skill of the three models is very similar. The indirect setup of the model, which means the prediction of the inundation state in summer via the water balance at the end of March, can be considered a major contributor to this outcome. Salt pans with a more balanced class distribution are more challenging to correctly estimate for the three models (Table 4.2). On average, the GROUNDWATER model performed best in predicting these eight salt pans (Zicklacke, Katschitzlacke, Fuchslochlacke 3, Oberer Stinkersee, Mittlerer Stinkersee, Wörtenlacken 2, Neubruchlacke, and Lange Lacke), although interpreting these results proved difficult due to the widely varying hydrological conditions of the salt pans (Krachler et al. 2012). Section 4.2.2 stresses the importance of the underlying physical conditions on the fold-wise performance. As already discussed in Section 5.1, moderate success mainly lies in the struggle to estimate extreme dry, and, especially, wet conditions in summer (e.g., drought around 1992, 2003, and 2016, and wet periods around especially 1996 (1997) and 2010).

As stated in Section 4.2.3, estimates were worse for years in which the inundation state shifted to the alternative state. The misclassifications are probably due to some salt pans reacting faster to hydrometeorological changes than others. Hence, for some salt pans, the environmental conditions of the previous months and year(s) have a stronger influence on the prediction of the current year than for others. Furthermore, the misclassifications may be partly due to the fact that the input features are coarse resolution (i.e., do not differ between Lacken) and partly to the model trying to get a best fit over all the years.

Although we did not apply feature selection (Jović et al. 2015) to reduce the number of features used in this study, we were able to inhibit overfitting in model testing. This was completed by trimming the decision trees used in the four RF models in the scope of the hyperparameter optimization. This built on our model design, which enables independent model testing and, practically, on closely monitoring training–test differences throughout this study.

In addition to changing climate patterns, a process referred to as “drying from beneath” (Krachler et al. 2000) challenges the water-holding capacity of the salt pans. Depending on the ecological state of the salt pans, this mechanism can directly influence WE and, therefore, the inundation state. We suppose that the worse the ecological health of the salt pan, the higher the negative impact on model performance. However, it is not possible to characterize this ecological state based on our models and using the available input data. Due to the skewed class distribution, the assumption that our predictor selection works better for more natural/ecologically healthy salt pans could not be answered inside this model setup. The disregarded large human influence on the water cycle (Zimmermann-Timm et al. 2021) constitutes an additional source of error.

All models are subject to a division between the periods before and after 2004 (Figure 4.3). This pattern cannot be found in the target variable (Figure 4.1). Additional research is needed to clearly connect climate change and the phenomenon of "dying salt pans" to these observations. As artificially inundated salt pans were introduced into the modeling, year-wise estimates could additionally have been affected due to misguided thresholding.

5.5 Model transferability

The model based on meteorological predictors can be transferred to any other salt pan ecosystem worldwide in combination with the use of high-resolution remote sensing imagery, such as that provided by Landsat. In general, globally available predictor data in sufficient temporal and spatial resolution with respect to the studied ecosystem are needed, at best in combination with uncertainty quantification. This can be ensured by choosing an adequate spatial resolution of the predictors with regard to the catchment size. Here, ERA5-Land offers a good starting point with its 9 km × 9 km spatial resolution. The EO data should have a suitable temporal and spatial resolution to capture the dynamics of the studied ecosystem. For example, it is not possible to retrieve the water extent information of ecosystems of a smaller size than the Landsat resolution of 30 m × 30 m. Another important constraint is that this approach will likely not be suitable in the case of water bodies whose water extent shows a low sensitivity with respect to water volume, i.e., with steep bathymetry in which a drop in the water level will not lead to a proportional decrease in the water area.

6. Conclusion and outlook

As salt pans in Seewinkel are increasingly vulnerable ecosystems in often poor hydrological conditions, we aimed at improving ecosystem understanding and, finally, decision-making by predicting the salt pan inundation state in summer and fall with ML models.

Our models stress the importance of groundwater for the estimation of the inundation state in summer/fall. This solidifies the general notion represented in the literature (Zimmermann-Timm et al. 2021; Krachler et al. 2012) and calls for sustainable groundwater management in the region to ensure the conservation of this ecosystem. We stress that the use of the SGI (Bloomfield et al. 2013) as a predictor is promising. The model based on meteorological predictors can be transferred to any other salt pan ecosystem worldwide in combination with the use of high-resolution remote sensing imagery, such as the Landsat archive. METEOROLOGY achieved an MCC of 0.66 compared to GROUNDWATER with 0.59 and COMBINED with 0.57, with respect to the independent test set. We identified the most likely sources of error, namely the struggle to estimate the inundation state correctly in the case of extreme environmental conditions developing after March, human intervention into the water cycle by artificially inundating the salt pans, and surface water loss due to the possible infiltration into deeper layers due to a failure of the water retention capacity (Krachler et al. 2000). Furthermore, we highlight the potential of the concept of partial dependency (Goldstein et al. 2015) to understand threshold-dependent ecosystems, such as salt pans in the Seewinkel region.

To our knowledge, the results represent the first data-driven prediction and understanding of salt pan dynamics in the Seewinkel region. We identified the main drivers and potential improvements for future model development. In this context, the use of more advanced ML algorithms could prove beneficial.

Furthermore, the possibility of transferring the METEOROLOGY model to other salt pan ecosystems in combination with EO data makes this study particularly valuable. We propose the application of our models to salt pans of larger sizes and ones that are less influenced by humans and in a better ecological condition. This could improve both performance and interpretability.

The possibility of predicting the salt pan inundation state in summer/fall is of potential importance to decision-makers in conservation and tourism (Dvorak et al. 2020; Krachler et al. 2012). A better understanding of salt pans can contribute to preserving this unique geographic space in the Pannonian Basin.

A. Appendix

Tab. A.1: Most important predictors for each salt pan according to PDP displayed together with the largest spread (in parentheses). Furthermore, the threshold for predicting a certain class for the most important predictor is indicated.

	Predictor with Largest PDP Spread	**Threshold for Predictor**
Badesee Apetlon	GW Anomal (0.18)	−0.09
Lange Lacke	SGI (0.51)	−0.09
Neubruchlacke	GW Anomal (0.43)	0.1
Kiesgrube	GW Anomal (0.12)	−0.12
Standlacke	GW Anomal (0.25)	0.14
Ochsenbrunnlacke	GW Anomal (0.25)	0.1
Gsigsee	GW Anomal (0.0)	−0.45
Wörtenlacken 2	SGI (0.61)	−0.03
Kirchsee	T Anomal (0.21)	−0.62
Wörtenlacken 1	GW Anomal (0.49)	−0.09
Mittlerer Stinkersee	SPI 24 (0.28)	0.09
Huldenlacke	T Anomal (0.13)	−0.2
Kleine Neubruchlacke	SPI 24 (0.21)	0.29
Heidlacke	GW Anomal (0.0)	−0.45
Unterer Stinkersee	SPI 24 (0.17)	−0.41
Sechsmahdlacke	GW Anomal (0.2)	0.14
Martenhofenlacke	SGI (0.22)	0.09
Oberer Stinkersee	SPI 24 (0.55)	0.29
Kuhbrunnlacke	GW Anomal (0.08)	0.1
Hottergrube	GW Anomal (0.0)	−0.45
Fuchslochlacke 3	SGI (0.32)	0.09
St. Martins Therme 2	SPI 24 (0.23)	−0.47
Fuchslochlacke 2	SGI (0.12)	0.09
St. Martins Therme 1	GW level ratio (0.15)	1.0
Fuchslochlacke 1	GW Anomal (0.31)	0.16
Hochstätten	P Anomal (0.16)	42.27
Herrnsee	SGI (0.33)	−0.03
Birnbaumlacke	SPI 24 (0.17)	0.73
Katschitzlacke	# Days ab. 25 °C (0.33)	64.0
Albersee	GW Anomal (0.21)	0.14
unbekannt	GW Anomal (0.08)	0.06
Zicksee	GW level ratio (0.09)	1.0
Darscholacke	GW Anomal (0.12)	−0.13
Zicklacke	SGI (0.59)	−0.03

Bibliography

Afrifa, S., T. Zhang, P. Appiahene, and V. Varadarajan (2022). "Mathematical and Machine Learning Models for Groundwater Level Changes: A Systematic Review and Bibliographic Analysis". In: *Future Internet* 14.9. ISSN: 1999-5903. DOI: 10.3390/fi14090259. URL: https://www.mdpi.com/1999-5903/14/9/259 (cit. on p. 3).

Ahmadi, A., M. Olyaei, Z. Heydari, M. Emami, A. Zeynolabedin, A. Ghomlaghi, A. Daccache, G. E. Fogg, and M. Sadegh (2022). "Groundwater Level Modeling with Machine Learning: A Systematic Review and Meta-Analysis". In: *Water* 14.6. ISSN: 2073-4441. DOI: 10.3390/w14060949. URL: https://www.mdpi.com/2073-4441/14/6/949 (cit. on p. 3).

Albert, R., V. Werner, M. Popp, M. Fischer, and H. Niklfeld (2020). "Botanische Kostbarkeiten vor unserer Haustür Die Salzpflanzen im Gebiet des Neusiedler Sees, Burgenland (Österreich)". In: *Acta ZooBot Austria* 157, pp. 115–143 (cit. on p. 1).

Altmann, A., L. Toloşi, O. Sander, and T. Lengauer (Apr. 2010). "Permutation importance: a corrected feature importance measure". In: *Bioinformatics* 26.10, pp. 1340–1347. ISSN: 1367-4803. DOI: 10.1093/bioinformatics/btq134. URL: 10.1093/bioinformatics/btq134 (cit. on pp. 20, 25).

Amin, R., R. Gould, W. Hou, R. Arnone, and Z. Lee (2012). "Optical algorithm for cloud shadow detection over water". In: *IEEE Transactions on Geoscience and Remote Sensing* 51.2, pp. 732–741 (cit. on p. 17).

Ardabili, S., A. Mosavi, M. Dehghani, and A. R. Várkonyi-Kóczy (2020). "Deep learning and machine learning in hydrological processes climate change and earth systems a systematic review". In: *Engineering for Sustainable Future: Selected papers of the 18th International Conference on Global Research and Education Inter-Academia–2019 18*. Springer. Berlin/Heidelberg, Germany, pp. 52–62. DOI: 10.1007/978-3-030-36841-8_5 (cit. on p. 3).

Bandhauer, M., F. Isotta, M. Lakatos, C. Lussana, L. Båserud, B. Izsák, O. Szentes, O. E. Tveito, and C. Frei (2022). "Evaluation of daily precipitation analyses in E-OBS (v19.0e) and ERA5 by comparison to regional high-resolution datasets in European regions". In: *International Journal of Climatology* 42.2, pp. 727–747. DOI: 10.1002/joc.7269. URL: https://rmets.onlinelibrary.wiley.com/doi/abs/10.1002/joc.7269 (cit. on p. 10).

Bartsch, A., A. M. Trofaier, G. Hayman, D. Sabel, S. Schlaffer, D. B. Clark, and E. Blyth (2012). "Detection of open water dynamics with ENVISAT ASAR in support of land surface modelling at high latitudes". In: *Biogeosciences* 9.2, pp. 703–714. DOI: 10.5194/bg-9-703-2012. URL: https://bg.copernicus.org/articles/9/703/2012/ (cit. on pp. 2, 18).

Belgiu, M. and L. Drăguţ (2016). "Random forest in remote sensing: A review of applications and future directions". In: *ISPRS Journal of Photogrammetry and Remote Sensing* 114, pp. 24–31. ISSN: 0924-2716. DOI: 10.1016/j.isprsjprs.2016.01.011. URL: https://www.sciencedirect.com/science/article/pii/S0924271616000265 (cit. on p. 19).

Bell, B., H. Hersbach, A. Simmons, P. Berrisford, P. Dahlgren, A. Horányi, J. Muñoz-Sabater, J. Nicolas, R. Radu, D. Schepers, C. Soci, S. Villaume, J.-R. Bidlot, L. Haimberger, J. Woollen, C. Buontempo, and J.-N. Thépaut (2021). "The ERA5 global reanalysis: Preliminary extension to 1950". In: *Quarterly Journal of the Royal Meteorological Society* 147.741, pp. 4186–4227. DOI: 10.1002/qj.4174. URL: https://rmets.onlinelibrary.wiley.com/doi/abs/10.1002/qj.4174 (cit. on p. 10).

Bergstra, J. and Y. Bengio (2012). "Random Search for Hyper-Parameter Optimization". In: *Journal of Machine Learning Research* 13.10, pp. 281–305. URL: http://jmlr.org/papers/v13/bergstra12a.html (cit. on p. 23).

Biau, G. and E. Scornet (Apr. 2016). "A random forest guided tour". In: *TEST* 25.2, pp. 197–227. DOI: 10.1007/s11749-016-0481-7 (cit. on pp. 19, 20).

Bioucas-Dias, J. M., A. Plaza, G. Camps-Valls, P. Scheunders, N. Nasrabadi, and J. Chanussot (2013). "Hyperspectral Remote Sensing Data Analysis and Future Challenges". In: *IEEE Geoscience and Remote Sensing Magazine* 1.2, pp. 6–36. DOI: 10.1109/MGRS.2013.2244672 (cit. on p. 14).

Birkett, C. (2000). "Synergistic Remote Sensing of Lake Chad: Variability of Basin Inundation". In: *Remote Sensing of Environment* 72.2, pp. 218–236. ISSN: 0034-4257. DOI: 10.1016/S0034-4257(99)00105-4. URL: https://www.sciencedirect.com/science/article/pii/S0034425799001054 (cit. on p. 18).

Bloch, M., L. Farkas, and K. Spiegler (1951). "Solar Evaporation of Salt Brines". In: *Industrial & Engineering Chemistry* 43.7, pp. 1544–1553. DOI: 10.1021/ie50499a025. URL: 10.1021/ie50499a025 (cit. on p. 9).

Bloomfield, J. P. and B. P. Marchant (2013). "Analysis of groundwater drought building on the standardised precipitation index approach". In: *Hydrology and Earth System Sciences* 17.12, pp. 4769–4787. DOI: 10.5194/hess-17-4769-2013. URL: https://hess.copernicus.org/articles/17/4769/2013/ (cit. on pp. 9, 10, 40, 45).

Blöschl, G. and M. Sivapalan (1995). "Scale issues in hydrological modelling: A review". In: *Hydrological Processes* 9.3-4, pp. 251–290. DOI: 10.1002/hyp.3360090305. URL: https://onlinelibrary.wiley.com/doi/abs/10.1002/hyp.3360090305 (cit. on p. 3).

Booysen, R., R. Gloaguen, S. Lorenz, R. Zimmermann, and P. A. Nex (2021). "Geological Remote Sensing". In: *Encyclopedia of Geology (Second Edition)*. Ed. by D. Alderton and S. A. Elias. Second Edition. Oxford: Academic Press, pp. 301–314. ISBN: 978-0-08-102909-1. DOI: 10.1016/B978-0-12-409548-9.12127-X. URL: https://www.sciencedirect.com/science/article/pii/B978012409548912127X (cit. on p. 14).

Boros, E., Z. Ecsedi, J. Oláh, R. Szegedi, and J. Dunn (2013). *Ecology and management of soda pans in the Carpathian Basin*. Hortobágy Environmental Association. ISBN: 9789630894715 (cit. on p. 1).

Boros, E., K. V.-Balogh, L. Vörös, and Z. Horváth (2017). "Multiple extreme environmental conditions of intermittent soda pans in the Carpathian Basin (Central Europe)". In: *Limnologica* 62, pp. 38–46. ISSN: 0075-9511. DOI: 10.1016/j.limno.2016.10.003. URL: https://www.sciencedirect.com/science/article/pii/S0075951116301815 (cit. on pp. 1, 2).

Bowen, B. B., E. L. Kipnis, and L. W. Raming (2017). "Temporal dynamics of flooding, evaporation, and desiccation cycles and observations of salt crust area change at the Bonneville Salt Flats, Utah". In: *Geomorphology* 299, pp. 1–11. DOI: 10.1016/j.geomorph.2017.09.036 (cit. on pp. 2, 13, 17).

Bowker, D. E. (1985). *Spectral reflectances of natural targets for use in remote sensing studies*. Vol. 1139. NASA (cit. on p. 14).

Breiman, L. (2001). "Random Forests". In: *Machine Learning* 45, pp. 5–32 (cit. on pp. 4, 19, 20, 23, 25).

Bryant, R. and M. Rainey (2002). "Investigation of flood inundation on playas within the Zone of Chotts, using a time-series of AVHRR". In: *Remote Sensing of Environment* 82.2, pp. 360–375. ISSN: 0034-4257. DOI: 10.1016/S0034-4257(02)00053-6. URL: https://www.sciencedirect.com/science/article/pii/S0034425702000536 (cit. on pp. 2, 13).

Bueechi, E., M. Fischer, L. Crocetti, M. Trnka, A. Grlj, L. Zappa, and W. Dorigo (2023). "Crop yield anomaly forecasting in the Pannonian basin using gradient boosting and its performance

in years of severe drought". In: *Agricultural and Forest Meteorology* 340, p. 109596. ISSN: 0168-1923. DOI: 10.1016/j.agrformet.2023.109596. URL: https://www.sciencedirect.com/science/article/pii/S0168192323002873 (cit. on p. 10).

Buitinck, L., G. Louppe, M. Blondel, F. Pedregosa, A. Mueller, O. Grisel, V. Niculae, P. Prettenhofer, A. Gramfort, J. Grobler, R. Layton, J. Vanderplas, A. Joly, B. Holt, and G. Varoquaux (2013). "API design for machine learning software: experiences from the scikit-learn project". In: *ArXiv*. DOI: 10.48550/arXiv.1309.0238 (cit. on p. 24).

Burgenland, L. (2016). *KLIMASZENARIEN FÜR DAS BUNDESLAND BURGENLAND BIS 2100*. Tech. rep. Eisenstadt, Austria, pp. 1–9 (cit. on p. 8).

Cabela, A., H. Grillitsch, and F. Tiedemann (2001). *Atlas zur Verbreitung und Ökologie der Amphibien und Reptilien in Österreich: Auswertung der Herpetofaunistischen Datenbank der Herpetologischen Sammlung des Naturhistorischen Museums in Wien*. Tech. rep. Umweltbundesamt, pp. 1–880 (cit. on p. 1).

Cancelliere, A. and J. D. Salas (2010). "Drought probabilities and return period for annual streamflows series". In: *Journal of Hydrology* 391.1, pp. 77–89. ISSN: 0022-1694. DOI: 10.1016/j.jhydrol.2010.07.008 (cit. on p. 40).

Cartwright, J., T. L. Morelli, and E. H. C. Grant (2022). "Identifying climate-resistant vernal pools: Hydrologic refugia for amphibian reproduction under droughts and climate change". In: *Ecohydrology* 15.5, e2354. DOI: 10.1002/eco.2354. URL: https://onlinelibrary.wiley.com/doi/abs/10.1002/eco.2354 (cit. on p. 4).

Castañeda, C., J. Herrero, and M. Auxiliadora Casterad (2005). "Landsat monitoring of playa-lakes in the Spanish Monegros desert". In: *Journal of Arid Environments* 63.2, pp. 497–516. ISSN: 0140-1963. DOI: 10.1016/j.jaridenv.2005.03.021. URL: https://www.sciencedirect.com/science/article/pii/S0140196305000728 (cit. on pp. 2, 13).

Cerqueira, V., L. Torgo, and I. Mozetič (Oct. 2020). "Evaluating time series forecasting models: An empirical study on performance estimation methods". In: *Machine Learning* 109, pp. 1997–2028. DOI: 10.1007/s10994-020-05910-7 (cit. on p. 23).

Chakraborty, S., R. Tomsett, R. Raghavendra, D. Harborne, M. Alzantot, F. Cerutti, M. Srivastava, A. Preece, S. Julier, R. M. Rao, T. D. Kelley, D. Braines, M. Sensoy, C. J. Willis, and P. Gurram (2017). "Interpretability of deep learning models: A survey of results". In: *2017 IEEE SmartWorld, Ubiquitous Intelligence Computing, Advanced Trusted Computed, Scalable Computing Communications, Cloud Big Data Computing, Internet of People and Smart City Innovation (SmartWorld/SCALCOM/UIC/ATC/CBDCom/IOP/SCI)*, pp. 1–6. DOI: 10.1109/UIC-ATC.2017.8397411 (cit. on p. 4).

Cheval, S. (2015). "The standardized precipitation index–an overview". In: *Rom. J. Meteorol* 12.1-2, pp. 17–64 (cit. on p. 11).

Chew, C. and E. Small (2020). "Estimating inundation extent using CYGNSS data: A conceptual modeling study". In: *Remote Sensing of Environment* 246, p. 111869. ISSN: 0034-4257. DOI: 10.1016/j.rse.2020.111869. URL: https://www.sciencedirect.com/science/article/pii/S003442572030239X (cit. on pp. 2, 13).

Chicco, D. and G. Jurman (Jan. 2020). "The advantages of the Matthews correlation coefficient (MCC) over F1 score and accuracy in binary classification evaluation". In: *BMC Genomics* 21. DOI: 10.1186/s12864-019-6413-7 (cit. on p. 25).

Chiloane, C., T. Dube, and C. Shoko (Oct. 2020). "Monitoring and assessment of the seasonal and inter-annual pan inundation dynamics in the Kgalagadi Transfrontier Park, Southern Africa". In: *Physics and Chemistry of the Earth, Parts A/B/C* 118-119, p. 102905. DOI: 10.1016/j.pce.2020.102905. URL: https://doi.org/10.1016%2Fj.pce.2020.102905 (cit. on pp. 2, 13, 17).

Choi, C., J. Kim, H. Han, D. Han, and H. S. Kim (2020). "Development of Water Level Prediction Models Using Machine Learning in Wetlands: A Case Study of Upo Wetland in South Korea". In: *Water* 12.1. ISSN: 2073-4441. DOI: 10.3390/w12010093. URL: https://www.mdpi.com/2073-4441/12/1/93 (cit. on p. 4).

Chouaib, W., Y. Alila, and P. V. Caldwell (2018). "Parameter transferability within homogeneous regions and comparisons with predictions from a priori parameters in the eastern United States". In: *Journal of Hydrology* 560, pp. 24–38. ISSN: 0022-1694. DOI: 10.1016/j.jhydrol.2018.03.018. URL: https://www.sciencedirect.com/science/article/pii/S0022169418301847 (cit. on p. 3).

Collenteur, R. A., M. Bakker, R. Caljé, S. A. Klop, and F. Schaars (2019). "Pastas: Open Source Software for the Analysis of Groundwater Time Series". In: *Groundwater* 57.6, pp. 877–885. DOI: 10.1111/gwat.12925. URL: https://ngwa.onlinelibrary.wiley.com/doi/abs/10.1111/gwat.12925 (cit. on p. 10).

Crocetti, L., M. Forkel, M. Fischer, F. Jurecka, A. Grlj, A. Salentinig, M. Trnka, M. Anderson, W.-T. Ng, Ž. Kokalj, A. Bucur, and W. Dorigo (Dec. 2020). "Earth Observation for agricultural drought monitoring in the Pannonian Basin (southeastern Europe): current state and future directions". In: *Regional Environmental Change* 20, p. 123. DOI: 10.1007/s10113-020-01710-w (cit. on pp. 7, 41).

Csaplovics, A., M. Götzinger, and C. Lengauer (Oct. 2018). "Die Salzminerale der Salzlacken im Seewinkel, Burgenland". In: *Mitteilungen der Österreichischen Mineralogischen Gesellschaft* 164, pp. 55–64. ISSN: 1609-0144 (cit. on p. 15).

Daniel, J., R. C. Rooney, and D. T. Robinson (2022). "Climate, land cover and topography: essential ingredients in predicting wetland permanence". In: *Biogeosciences* 19.5, pp. 1547–1570. DOI: 10.5194/bg-19-1547-2022. URL: https://bg.copernicus.org/articles/19/1547/2022/ (cit. on pp. 4, 8).

Dickerson, R. and A. Forman (Feb. 2014). *Surface Geology, Paleoenvironment, and Paleoclimate of Stonewall Mountain, Nellis Air Force Base, Nevada*. Tech. rep., pp. 1–250 (cit. on p. 15).

Dorigo, W., S. Dietrich, F. Aires, L. Brocca, S. Carter, J.-F. Cretaux, D. Dunkerley, H. Enomoto, R. Forsberg, A. Güntner, M. I. Hegglin, R. Hollmann, D. F. Hurst, J. A. Johannessen, C. Kummerow, T. Lee, K. Luojus, U. Looser, D. G. Miralles, V. Pellet, T. Recknagel, C. R. Vargas, U. Schneider, P. Schoeneich, M. Schröder, N. Tapper, V. Vuglinsky, W. Wagner, L. Yu, L. Zappa, M. Zemp, and V. Aich (2021). "Closing the Water Cycle from Observations across Scales: Where Do We Stand?" In: *Bulletin of the American Meteorological Society* 102.10, E1897–E1935. DOI: 10.1175/BAMS-D-19-0316.1. URL: https://journals.ametsoc.org/view/journals/bams/102/10/BAMS-D-19-0316.1.xml (cit. on p. 4).

Dorigo, W., A. Lucieer, T. Podobnikar, and A. Čarni (2012). "Mapping invasive Fallopia japonica by combined spectral, spatial, and temporal analysis of digital orthophotos". In: *International Journal of Applied Earth Observation and Geoinformation* 19, pp. 185–195. ISSN: 1569-8432. DOI: 10.1016/j.jag.2012.05.004. URL: https://www.sciencedirect.com/science/article/pii/S0303243412001122 (cit. on p. 19).

Doxaran, D., J.-M. Froidefond, S. Lavender, and P. Castaing (2002). "Spectral signature of highly turbid waters: Application with SPOT data to quantify suspended particulate matter concentrations". In: *Remote Sensing of Environment* 81.1, pp. 149–161. ISSN: 0034-4257. DOI: 10.1016/S0034-4257(01)00341-8. URL: https://www.sciencedirect.com/science/article/pii/S0034425701003418 (cit. on p. 13).

Draganits, E., M. Weißl, A. Zámolyi, and M. Doneus (2022). "Lake Neusiedl area: A particular lakescape at the boundary between Alps and Pannonian Basin". In: *Landscapes and Landforms of Austria*. Berlin/Heidelberg, Germany: Springer, pp. 207–222 (cit. on p. 7).

Dvorak, M., G. Bieringer, B. Braun, A. Grüll, E. Karner-Ranner, B. Kohler, I. Korner, J. Laber, E. Nemeth, G. Rauer, and B. Wendelin (2016). "Population size, distribution and population trends of threatened and ecologically important bird species in the National Park Neusiedler See - Seewinkel: results from the years 2001-2015". In: *Egretta* 54, pp. 4–86 (cit. on pp. 1, 21).

Dvorak, M., J. Laber, A. Ranner, A. Pellinger, S. Tatai, T. Hadarics, C. Dorogman, and A. Lang (2020). *Artenliste der Avifauna des Neusiedler See - Gebiets*. Tech. rep. Nationalpark Neusiedler See - Seewinkel Fertő–Hanság Nemzeti Park BirdLife Österreich, pp. 1–92. URL: https://www.nationalparkneusiedlersee.at/media/2279/2021-02-25-04-np-artenliste_booklet__online-interaktiv__lowres.pdf (cit. on pp. 1, 21, 45).

Dvorak, M., A. Landmann, N. Teufelbauer, G. Wichmann, H.-M. Berg, and R. Probst (2017). "The conservation status of the breeding birds of Austria: Red List (5th version) and Birds of Conservation Concern (1st version)". In: *Egretta* 55, pp. 6–42 (cit. on p. 1).

Eitzinger, J., G. Kubu, H. Formayer, P. Haas, T. Gerersdorfer, and H. Kromp-Kolb (2005). *Auswirkungen einer Klimaänderung auf den Wasserhaushalt des Neusiedlersees*. Tech. rep. (cit. on p. 7).

Faddoul, J. B., B. Chidlovskii, R. Gilleron, and F. Torre (2012). "Learning Multiple Tasks with Boosted Decision Trees". In: *Proceedings of the 2012th European Conference on Machine Learning and Knowledge Discovery in Databases - Volume Part I*. ECMLPKDD'12. Bristol, UK: Springer-Verlag, pp. 681–696. ISBN: 9783642334597 (cit. on p. 20).

Fahimi, F., Z. M. Yaseen, and A. El-shafie (2017). "Application of soft computing based hybrid models in hydrological variables modeling: a comprehensive review". In: *Theoretical and applied climatology* 128, pp. 875–903. DOI: 10.1007/s00704-016-1735-8 (cit. on p. 4).

Farmer, W. H. and R. M. Vogel (2016). "On the deterministic and stochastic use of hydrologic models". In: *Water Resources Research* 52.7, pp. 5619–5633. DOI: 10.1002/2016WR019129. URL: https://agupubs.onlinelibrary.wiley.com/doi/abs/10.1002/2016WR019129 (cit. on p. 3).

Ferreira, J. A. (2022). *Models under which random forests perform badly; consequences for applications* (cit. on p. 20).

Feyisa, G. L., H. Meilby, R. Fensholt, and S. R. Proud (2014). "Automated Water Extraction Index: A new technique for surface water mapping using Landsat imagery". In: *Remote sensing of environment* 140, pp. 23–35 (cit. on p. 17).

Foti, R., M. del Jesus, A. Rinaldo, and I. Rodriguez-Iturbe (2012). "Hydroperiod regime controls the organization of plant species in wetlands". In: *Proceedings of the National Academy of Sciences* 109.48, pp. 19596–19600. DOI: 10.1073/pnas.1218056109. URL: https://www.pnas.org/doi/abs/10.1073/pnas.1218056109 (cit. on p. 2).

Friedman, J. H. (2001). "Greedy function approximation: A gradient boosting machine." In: *The Annals of Statistics* 29.5, pp. 1189–1232. DOI: 10.1214/aos/1013203451 (cit. on pp. 20, 25).

Fukunaga, K. and D. Hummels (1989). "Leave-one-out procedures for nonparametric error estimates". In: *IEEE Transactions on Pattern Analysis and Machine Intelligence* 11.4, pp. 421–423. DOI: 10.1109/34.19039 (cit. on pp. 22, 25).

Gitelson, A. A. and M. N. Merzlyak (1996). "Signature analysis of leaf reflectance spectra: algorithm development for remote sensing of chlorophyll". In: *Journal of plant physiology* 148.3-4, pp. 494–500 (cit. on p. 15).

Gitelson, A. A. and M. N. Merzlyak (1998). "Remote sensing of chlorophyll concentration in higher plant leaves". In: *Advances in Space Research* 22.5, pp. 689–692 (cit. on p. 15).

Goldstein, A., A. Kapelner, J. Bleich, and E. Pitkin (2015). "Peeking Inside the Black Box: Visualizing Statistical Learning With Plots of Individual Conditional Expectation". In: *Journal of Computational and Graphical Statistics* 24.1, pp. 44–65. DOI: 10.1080/10618600.2014.907095 (cit. on pp. 20, 25, 45).

Gunning, D., M. Stefik, J. Choi, T. Miller, S. Stumpf, and G.-Z. Yang (2019). "XAI—Explainable artificial intelligence". In: *Science robotics* 4.37, eaay7120. DOI: 10.1126/scirobotics.aay7120 (cit. on p. 5).

Hackl, P. and J. Ledolter (Mar. 2023). "A Statistical Analysis of the Water Levels at Lake Neusiedl". In: *Austrian Journal of Statistics* 52.1, pp. 87–100. DOI: 10.17713/ajs.v52i1.1444. URL: https://www.ajs.or.at/index.php/ajs/article/view/1444 (cit. on pp. 7, 41).

Hamed, K. H. and A. R. Rao (1998). "A modified Mann-Kendall trend test for autocorrelated data". In: *Journal of hydrology* 204.1-4, pp. 182–196 (cit. on p. 8).

Harris, C. R., K. J. Millman, S. J. Van Der Walt, R. Gommers, P. Virtanen, D. Cournapeau, E. Wieser, J. Taylor, S. Berg, N. J. Smith, et al. (2020). "Array programming with NumPy". In: *Nature* 585.7825, pp. 357–362. DOI: 10.1038/s41586-020-2649-2 (cit. on pp. 10, 11).

Haslinger, K., W. Schöner, J. Abermann, G. Laaha, K. Andre, M. Olefs, and R. Koch (2023). "Apparent contradiction in the projected climatic water balance for Austria: wetter conditions on average versus higher probability of meteorological droughts". In: *Natural Hazards and Earth System Sciences* 23, pp. 2749–2768. DOI: 10.5194/nhess-23-2749-2023 (cit. on p. 8).

Hastie, T., R. Tibshirani, and J. Friedman (2001). *The Elements of Statistical Learning*. Springer Series in Statistics. New York, NY, USA: Springer New York Inc. (cit. on pp. 19, 20).

Häusler, H. (2007). "Erläuterungen zu den Blättern 79 Neusiedl am See 80 Ungarisch-Altenburg 109 Pamhagen". In: *Geologische Karte der Republik Österreich 1 : 50 000*. Ed. by G. Bundesanstalt, pp. 145–157 (cit. on p. 7).

Häusler, H. (2020). "Wie gelangte das Salz in die Salzlacken? – Zum Stand der Forschung über die Entstehung des „Salzführenden Horizontes" und der Salzböden des Seewinkels". In: *Acta ZooBot Austria* 157, pp. 145–157 (cit. on p. 7).

Heintzman, L., S. Starr, K. Mulligan, L. Barbato, and N. McIntyre (Aug. 2017). "Using Satellite Imagery to Examine the Relationship between Surface-Water Dynamics of the Salt Lakes of Western Texas and Ogallala Aquifer Depletion". In: *Wetlands* 37, pp. 1–11. DOI: 10.1007/s13157-017-0940-2 (cit. on pp. 2, 13).

Hersbach, H., B. Bell, P. Berrisford, S. Hirahara, A. Horányi, J. Muñoz-Sabater, J. Nicolas, C. Peubey, R. Radu, D. Schepers, A. Simmons, C. Soci, S. Abdalla, X. Abellan, G. Balsamo, P. Bechtold, G. Biavati, J. Bidlot, M. Bonavita, G. De Chiara, P. Dahlgren, D. Dee, M. Diamantakis, R. Dragani, J. Flemming, R. Forbes, M. Fuentes, A. Geer, L. Haimberger, S. Healy, R. J. Hogan, E. Hólm, M. Janisková, S. Keeley, P. Laloyaux, P. Lopez, C. Lupu, G. Radnoti, P. de Rosnay, I. Rozum, F. Vamborg, S. Villaume, and J.-N. Thépaut (2020). "The ERA5 global reanalysis". In: *Quarterly Journal of the Royal Meteorological Society* 146.730, pp. 1999–2049. DOI: 10.1002/qj.3803 (cit. on p. 10).

Herzig, A. (2020). "Soda pans – jewels of the Nationalpark Neusiedler See-Seewinkel An opinion based on limnological data". In: *Acta ZooBot Austria* 157, pp. 81–114 (cit. on p. 1).

Hess, L. L., J. M. Melack, E. M. Novo, C. C. Barbosa, and M. Gastil (2003). "Dual-season mapping of wetland inundation and vegetation for the central Amazon basin". In: *Remote Sensing of Environment* 87.4. Large Scale Biosphere Atmosphere Experiment in Amazonia, pp. 404–428. ISSN: 0034-4257. DOI: 10.1016/j.rse.2003.04.001. URL: https://www.sciencedirect.com/science/article/pii/S0034425703002025 (cit. on pp. 2, 13, 18).

Horváth, Z., R. Ptacnik, C. F. Vad, and J. M. Chase (Apr. 2019). "Habitat loss over six decades accelerates regional and local biodiversity loss via changing landscape connectance". In: *Ecology Letters* 22.6. Ed. by T. Coulson, pp. 1019–1027. DOI: 10.1111/ele.13260. URL: https://www.ncbi.nlm.nih.gov/pmc/articles/PMC6518933 (cit. on p. 1).

Hughes, A., M. Mansour, R. Ward, N. Kieboom, S. Allen, D. Seccombe, M. Charlton, and C. Prudhomme (2021). "The impact of climate change on groundwater recharge: National-scale assessment for the British mainland". In: *Journal of Hydrology* 598, p. 126336. ISSN: 0022-1694.

DOI: 10.1016/j.jhydrol.2021.126336. URL: https://www.sciencedirect.com/science/article/pii/S0022169421003838 (cit. on p. 9).

Hunter, J. D. (2007). "Matplotlib: A 2D graphics environment". In: *Computing in science & engineering* 9.03, pp. 90–95. DOI: 10.1109/MCSE.2007.55 (cit. on p. 19).

Hussaini, A., M. R. Mahmud, K. T. K. Wee, and A. G. Abubakar (2020). "A Review of Water Level Fluctuation Models and Modelling Initiatives". In: *Journal of Computational and Theoretical Nanoscience* 17.2-3, pp. 645–653. ISSN: 1546-1955. DOI: doi:10.1166/jctn.2020.8781. URL: https://www.ingentaconnect.com/content/asp/jctn/2020/00000017/00000002/art00014 (cit. on p. 4).

Jajarmizadeh, M. (Jan. 2012). "A Review on Theoretical Consideration and Types of Models in Hydrology". In: *Journal of Environmental Science and Technology* 5, pp. 249–261. DOI: 10.3923/jest.2012.249.261 (cit. on p. 3).

Jensen, J. (2007). *Remote Sensing of the Environment: An Earth Resource Perspective*. Prentice Hall series in geographic information science. Pearson Prentice Hall. ISBN: 9780131889507. URL: https://books.google.de/books?id=A6YsAQAAMAAJ (cit. on pp. 13–15, 17).

Ji, L., L. Zhang, and B. Wylie (2009). "Analysis of dynamic thresholds for the normalized difference water index". In: *Photogrammetric Engineering & Remote Sensing* 75.11, pp. 1307–1317 (cit. on p. 16).

Jones, J. (2019). "Improved Automated Detection of Subpixel-Scale Inundation—Revised Dynamic Surface Water Extent (DSWE) Partial Surface Water Tests". In: *Remote Sensing* 11.4. ISSN: 2072-4292. DOI: 10.3390/rs11040374. URL: https://www.mdpi.com/2072-4292/11/4/374 (cit. on p. 2).

Joseph, V. R. (Apr. 2022). "Optimal ratio for data splitting". In: *Statistical Analysis and Data Mining: The ASA Data Science Journal* 15.4, pp. 531–538. DOI: 10.1002/sam.11583. URL: https://onlinelibrary.wiley.com/doi/abs/10.1002/sam.11583 (cit. on p. 21).

Jović, A., K. Brkić, and N. Bogunović (2015). "A review of feature selection methods with applications". In: *2015 38th International Convention on Information and Communication Technology, Electronics and Microelectronics (MIPRO)*, pp. 1200–1205. DOI: 10.1109/MIPRO.2015.7160458 (cit. on pp. 8, 42).

Ju, J. and D. P. Roy (2008). "The availability of cloud-free Landsat ETM+ data over the conterminous United States and globally". In: *Remote Sensing of Environment* 112.3, pp. 1196–1211 (cit. on p. 17).

Justice, C., E. Vermote, J. Townshend, R. Defries, D. Roy, D. Hall, V. Salomonson, J. Privette, G. Riggs, A. Strahler, W. Lucht, R. Myneni, Y. Knyazikhin, S. Running, R. Nemani, Z. Wan, A. Huete, W. van Leeuwen, R. Wolfe, L. Giglio, J. Muller, P. Lewis, and M. Barnsley (1998). "The Moderate Resolution Imaging Spectroradiometer (MODIS): land remote sensing for global change research". In: *IEEE Transactions on Geoscience and Remote Sensing* 36.4, pp. 1228–1249. DOI: 10.1109/36.701075 (cit. on p. 2).

Kerekes, J. P. (2008). "Optical Sensor Technology". In: *The SAGE Handbook of Remote Sensing*. SAGE Publications, Inc., pp. 94–107. DOI: 10.4135/9780857021052.n7. URL: https://doi.org/10.4135%2F9780857021052.n7 (cit. on p. 14).

Khandelwal, A., S. Xu, X. Li, X. Jia, M. Stienbach, C. Duffy, J. Nieber, and V. Kumar (2020). *Physics Guided Machine Learning Methods for Hydrology* (cit. on p. 4).

Kirschner, A., R. Krachler, R. Krachler, and I. Korner (2007). *Renaturierung ausgewählter Salzlacken des burgenländischen Seewinkels*. Tech. rep. 1-2. Naturschutzbund Burgenland, pp. 23–27 (cit. on p. 7).

Kokaly, R., R. Clark, G. Swayze, K. Livo, T. Hoefen, N. Pearson, R. Wise, W. Benzel, H. Lowers, R. Driscoll, et al. (2017). "Usgs spectral library version 7 data: Us geological survey data release". In: *United States Geological Survey (USGS): Reston, VA, USA* 61 (cit. on pp. 14, 16).

Köppen, W. (June 2011). "The thermal zones of the Earth according to the duration of hot, moderate and cold periods and to the impact of heat on the organic world". In: *Meteorologische Zeitschrift* 20.3, pp. 351–360. DOI: 10.1127/0941-2948/2011/105. URL: http://dx.doi.org/10.1127/0941-2948/2011/105 (cit. on p. 7).

Kornfeld, R. P., B. W. Arnold, M. A. Gross, N. T. Dahya, W. M. Klipstein, P. F. Gath, and S. Bettadpur (2019). "GRACE-FO: The Gravity Recovery and Climate Experiment Follow-On Mission". In: *Journal of Spacecraft and Rockets* 56.3, pp. 931–951. DOI: 10.2514/1.A34326. URL: 10.2514/1.A34326 (cit. on p. 18).

Krachler, R., I. Korner, M. Dvorak, N. Milazowszky, W. Rabitsch, F. Werba, P. Zulka, and A. Kirschner (2012). *Die Salzlacken des Seewinkels: Erhebung des aktuellen oekologischen Zustandes sowie Entwicklung individueller Lackenerhaltungskonzepte fuer die Salzlacken des Seewinkels (2008-2011)*. Tech. rep. Naturschutzbund Burgenland (cit. on pp. 1, 2, 7, 9, 14, 19–21, 39–42, 45).

Krachler, R., R. Krachler, E. Milleret, and W. Wesner (2000). "Limnochemische Untersuchungen zur aktuellen Situation der Salzlacken im burgenlaendischen Seewinkel". In: *Burgenlaendische Heimatblaetter* 62, pp. 1–48 (cit. on pp. 1, 2, 7, 9, 18, 42, 45).

Krachler, R. (2007). *Renaturierung von Sodalacken im burgenländischen Seewinkel* (cit. on pp. 9, 15).

Kraft, B., M. Jung, M. Körner, S. Koirala, and M. Reichstein (2022). "Towards hybrid modeling of the global hydrological cycle". In: *Hydrology and Earth System Sciences* 26.6, pp. 1579–1614. DOI: 10.5194/hess-26-1579-2022. URL: https://hess.copernicus.org/articles/26/1579/2022/ (cit. on p. 4).

Krzepek, K., J. Schmidt, and D. Iwaszczuk (2022). "Fusion of SAR and Multi-spectral Time Series for Determination of Water Table Depth and Lake Area in Peatlands". In: *PFG–Journal of Photogrammetry, Remote Sensing and Geoinformation Science* 90.6, pp. 561–575 (cit. on p. 2).

Kseňak, Ľ., K. Pukanská, K. Bartoš, and P. Blišťan (2022). "Assessment of the Usability of SAR and Optical Satellite Data for Monitoring Spatio-Temporal Changes in Surface Water: Bodrog River Case Study". In: *Water* 14.3. ISSN: 2073-4441. DOI: 10.3390/w14030299. URL: https://www.mdpi.com/2073-4441/14/3/299 (cit. on p. 2).

Kumar, R., J. L. Musuuza, A. F. Van Loon, A. J. Teuling, R. Barthel, J. Ten Broek, J. Mai, L. Samaniego, and S. Attinger (2016). "Multiscale evaluation of the Standardized Precipitation Index as a groundwater drought indicator". In: *Hydrology and Earth System Sciences* 20.3, pp. 1117–1131. DOI: 10.5194/hess-20-1117-2016. URL: https://hess.copernicus.org/articles/20/1117/2016/ (cit. on p. 9).

Landgrebe, D. A. (2003). *Signal theory methods in multispectral remote sensing*. Vol. 24. John Wiley & Sons (cit. on p. 14).

Lange, H. and S. Sippel (Feb. 2020). "Machine Learning Applications in Hydrology". In: *Forest-Water Interactions*. Ed. by D. F. Levia, D. E. Carlyle-Moses, S. Iida, B. Michalzik, K. Nanko, and A. Tischer. Vol. 240. Cham: Springer International Publishing, pp. 233–257. ISBN: 978-3-030-26085-9. DOI: 10.1007/978-3-030-26086-6_10. URL: https://doi.org/10.1007/978-3-030-26086-6_10 (cit. on p. 3).

Lavers, D. A., A. Simmons, F. Vamborg, and M. J. Rodwell (2022). "An evaluation of ERA5 precipitation for climate monitoring". In: *Quarterly Journal of the Royal Meteorological Society* 148.748, pp. 3152–3165. DOI: 10.1002/qj.4351. URL: https://rmets.onlinelibrary.wiley.com/doi/abs/10.1002/qj.4351 (cit. on p. 10).

Le Vine, D. and N. Skou (2006). *Microwave radiometer systems: design and analysis*. Artech (cit. on p. 18).

LeCun, Y., Y. Bengio, and G. Hinton (May 2015). "Deep learning". In: *Nature* 521.7553, pp. 436–444. DOI: 10.1038/nature14539. URL: https://doi.org/10.1038%2Fnature14539 (cit. on p. 4).

Leemans, R. and R. De Groot (2003). *Millennium Ecosystem Assessment: Ecosystems and human well-being: a framework for assessment*. Island press (cit. on p. 1).

Lefebvre, G., A. Davranche, L. Willm, J. Campagna, L. Redmond, C. Merle, A. Guelmami, and B. Poulin (2019). "Introducing WIW for Detecting the Presence of Water in Wetlands with Landsat and Sentinel Satellites". In: *Remote Sensing* 11.19. ISSN: 2072-4292. DOI: 10.3390/rs11192210. URL: https://www.mdpi.com/2072-4292/11/19/2210 (cit. on pp. 2, 13).

Li, B., G. Yang, R. Wan, X. Dai, and Y. Zhang (July 2016). "Comparison of random forests and other statistical methods for the prediction of lake water level: a case study of the Poyang Lake in China". In: *Hydrology Research* 47.S1, pp. 69–83. ISSN: 0029-1277. DOI: 10.2166/nh.2016.264. URL: 10.2166/nh.2016.264 (cit. on p. 4).

Li, C. Z., L. Zhang, H. Wang, Y. Q. Zhang, F. L. Yu, and D. H. Yan (2012). "The transferability of hydrological models under nonstationary climatic conditions". In: *Hydrology and Earth System Sciences* 16.4, pp. 1239–1254. DOI: 10.5194/hess-16-1239-2012. URL: https://hess.copernicus.org/articles/16/1239/2012/ (cit. on p. 3).

Li, H., D. Mao, X. Li, Z. Wang, and C. Wang (2019). "Monitoring 40-Year Lake Area Changes of the Qaidam Basin, Tibetan Plateau, Using Landsat Time Series". In: *Remote Sensing* 11.3. ISSN: 2072-4292. DOI: 10.3390/rs11030343. URL: https://www.mdpi.com/2072-4292/11/3/343 (cit. on pp. 2, 13).

Li, X., F. Ling, X. Cai, Y. Ge, X. Li, Z. Yin, C. Shang, X. Jia, and Y. Du (Dec. 2021). "Mapping water bodies under cloud cover using remotely sensed optical images and a spatiotemporal dependence model". In: *International Journal of Applied Earth Observation and Geoinformation* 103, p. 102470. DOI: 10.1016/j.jag.2021.102470. URL: https://doi.org/10.1016%2Fj.jag.2021.102470 (cit. on p. 17).

Linusson, H. (2013). "Multi-output random forests". In: University of Borås/School of Business and IT. URL: https://api.semanticscholar.org/CorpusID:122685952 (cit. on p. 20).

Liu, G. and F. W. Schwartz (Feb. 2011). "An integrated observational and model-based analysis of the hydrologic response of prairie pothole systems to variability in climate". In: *Water Resources Research* 47.2. DOI: 10.1029/2010wr009084. URL: https://doi.org/10.1029%2F2010wr009084 (cit. on pp. 3, 41).

Liu, T., C. J. Harman, E. L. Kipnis, and B. B. Bowen (2017). "Modeling Episodic Ephemeral Brine Lake Evaporation and Salt Crystallization on the Bonneville Salt Flats, Utah". In: *AGU Fall Meeting Abstracts* (New Orleans, USA, Dec. 11–15, 2017). Vol. 2017, EP11C–1568 (cit. on p. 9).

Liu, Z., Y. Wang, Z. Xu, and Q. Duan (2017). "Conceptual Hydrological Models". In: *Handbook of Hydrometeorological Ensemble Forecasting*. Ed. by Q. Duan, F. Pappenberger, J. Thielen, A. Wood, H. L. Cloke, and J. C. Schaake. Berlin, Heidelberg: Springer Berlin Heidelberg, pp. 1–23. ISBN: 978-3-642-40457-3. DOI: 10.1007/978-3-642-40457-3_22-1. URL: 10.1007/978-3-642-40457-3_22-1 (cit. on p. 3).

Lodhi, M. A., D. C. Rundquist, L. Han, and M. S. Kuzila (Feb. 1997). "THE POTENTIAL FOR REMOTE SENSING OF LOESS SOILS SUSPENDED IN SURFACE WATERSsup1/sup". In: *JAWRA Journal of the American Water Resources Association* 33.1, pp. 111–117. DOI: 10.1111/j.1752-1688.1997.tb04087.x. URL: https://doi.org/10.1111%2Fj.1752-1688.1997.tb04087.x (cit. on p. 14).

Lorena, A., L. P. Garcia, J. Lehmann, M. de Souto, and T. Ho (Sept. 2019). "How Complex Is Your Classification Problem?: A Survey on Measuring Classification Complexity". In: *ACM Computing Surveys* 52, pp. 1–34. DOI: 10.1145/3347711 (cit. on p. 19).

Lowenstein, T. K. and L. A. Hardie (1985). "Criteria for the recognition of salt-pan evaporites". In: *Sedimentology* 32.5, pp. 627–644. DOI: 10.1111/j.1365-3091.1985.tb00478.x. URL: https://onlinelibrary.wiley.com/doi/abs/10.1111/j.1365-3091.1985.tb00478.x (cit. on pp. 1, 8, 9, 21).

McFeeters, S. K. (1996). "The use of the Normalized Difference Water Index (NDWI) in the delineation of open water features". In: *International Journal of Remote Sensing* 17 (7), pp. 1425–1432. ISSN: 13665901. DOI: 10.1080/01431169608948714 (cit. on p. 16).

McKee, T. B., N. J. Doesken, J. Kleist, et al. (1993). "The relationship of drought frequency and duration to time scales". In: *Proceedings of the 8th Conference on Applied Climatology*. Vol. 17. 22. California, pp. 179–183 (cit. on pp. 9, 11, 40).

Miralles, D. G., R. A. M. De Jeu, J. H. Gash, T. R. H. Holmes, and A. J. Dolman (2011). "Magnitude and variability of land evaporation and its components at the global scale". In: *Hydrology and Earth System Sciences* 15.3, pp. 967–981. DOI: 10.5194/hess-15-967-2011 (cit. on p. 40).

Mitter, H. and E. Schmid (2021). "Informing groundwater policies in semi-arid agricultural production regions under stochastic climate scenario impacts". In: *Ecological Economics* 180, p. 106908. ISSN: 0921-8009. DOI: 10.1016/j.ecolecon.2020.106908. URL: https://www.sciencedirect.com/science/article/pii/S0921800920321996 (cit. on pp. 1, 7).

Molnar, C. (2020). *Interpretable machine learning*. Lulu.com (cit. on p. 25).

Morgenthaler, S. (2009). "Exploratory data analysis". In: *WIREs Computational Statistics* 1.1, pp. 33–44. DOI: 10.1002/wics.2. URL: https://wires.onlinelibrary.wiley.com/doi/abs/10.1002/wics.2 (cit. on p. 19).

Mosaffa, H., M. Sadeghi, I. Mallakpour, M. Naghdyzadegan Jahromi, and H. R. Pourghasemi (2022). "Chapter 43 - Application of machine learning algorithms in hydrology". In: *Computers in Earth and Environmental Sciences*. Ed. by H. R. Pourghasemi. Amsterdam, The Netherlands: Elsevier, pp. 585–591. ISBN: 978-0-323-89861-4. DOI: 10.1016/B978-0-323-89861-4.00027-0. URL: https://www.sciencedirect.com/science/article/pii/B9780323898614000270 (cit. on p. 3).

Mougenot, B., M. Pouget, and G. Epema (Jan. 1993). "Remote sensing of salt affected soils". In: *Remote Sensing Reviews* 7 (cit. on p. 15).

Muñoz-Sabater, J., E. Dutra, A. Agustı-Panareda, C. Albergel, G. Arduini, G. Balsamo, S. Boussetta, M. Choulga, S. Harrigan, H. Hersbach, B. Martens, D. G. Miralles, M. Piles, N. J. Rodrıguez-Fernández, E. Zsoter, C. Buontempo, and J.-N. Thépaut (2021). "ERA5-Land: a state-of-the-art global reanalysis dataset for land applications". In: *Earth System Science Data* 13.9, pp. 4349–4383. DOI: 10.5194/essd-13-4349-2021. URL: https://essd.copernicus.org/articles/13/4349/2021/ (cit. on pp. 4, 9–11).

Mustard, J., M. Staid, and W. Fripp (Mar. 2001). "A Semianalytical Approach to the Calibration of AVIRIS Data to Reflectance over Water". In: *Remote Sensing of Environment* 75, pp. 335–349. DOI: 10.1016/S0034-4257(00)00177-2 (cit. on p. 13).

Nationalpark Neusiedler See - Seewinkel (2022). *Lackenbecken, eigene Daten* (cit. on p. 3).

Nayak, S., A. Pandeya, M. Gupta, C. Trivedi, K. Prasad, and S. Kadri (1989). "APPLICATION OF SATELLITE DATA FOR MONITORING DEGRADATION OF TIDAL WETLANDS OF THE GULF OF KACHCHH, WESTERN INDIA". In: *Space and Humanity*. Elsevier, pp. 171–178. DOI: 10.1016/b978-0-08-037877-0.50024-7. URL: https://doi.org/10.1016%2Fb978-0-08-037877-0.50024-7 (cit. on p. 1).

Nearing, G. S., F. Kratzert, A. K. Sampson, C. S. Pelissier, D. Klotz, J. M. Frame, C. Prieto, and H. V. Gupta (Mar. 2021). "What Role Does Hydrological Science Play in the Age of Machine Learning?" In: *Water Resources Research* 57.3. DOI: 10.1029/2020wr028091. URL: https://doi.org/10.1029%2F2020wr028091 (cit. on p. 3).

Nhiwatiwa, T. and T. Dalu (Feb. 2017). "Seasonal variation in pans in relation to limno-chemistry, size, hydroperiod, and river connectivity in a semi-arid subtropical region". In: *Physics and Chemistry of the Earth, Parts A/B/C* 97, pp. 37–45. DOI: 10.1016/j.pce.2016.11.003. URL: https://doi.org/10.1016%2Fj.pce.2016.11.003 (cit. on p. 2).

Nistor, M.-M., S. Cheval, A. F. Gualtieri, A. Dumitrescu, V. E. Boţan, A. Berni, G. Hognogi, I. A. Irimuş, and C. G. Porumb-Ghiurco (2017). "Crop evapotranspiration assessment under climate change in the Pannonian basin during 1991–2050". In: *Meteorological Applications* 24.1, pp. 84–91. DOI: 10.1002/met.1607. URL: https://rmets.onlinelibrary.wiley.com/doi/abs/10.1002/met.1607 (cit. on p. 11).

Nourani, V., A. Hosseini Baghanam, J. Adamowski, and O. Kisi (2014). "Applications of hybrid wavelet–Artificial Intelligence models in hydrology: A review". In: *Journal of Hydrology* 514, pp. 358–377. ISSN: 0022-1694. DOI: 10.1016/j.jhydrol.2014.03.057. URL: https://www.sciencedirect.com/science/article/pii/S002216941400242X (cit. on p. 4).

Opitz, J. and S. Burst (2019). "Macro f1 and macro f1". In: *arXiv*. DOI: 10.48550/arXiv.1911.03347 (cit. on p. 25).

Oroud, I. (1999). "Temperature and evaporation dynamics of saline solutions". In: *Journal of Hydrology* 226.1, pp. 1–10. ISSN: 0022-1694. DOI: 10.1016/S0022-1694(99)00138-9 (cit. on p. 9).

Oroud, I. (2001). "Dynamics of evaporation from saline water bodies". In: *Journal of Geophysical Research: Atmospheres* 106.D5, pp. 4695–4701. DOI: 10.1029/2000JD900061 (cit. on p. 9).

Osman, A. I. A., A. N. Ahmed, Y. F. Huang, P. Kumar, A. H. Birima, M. Sherif, A. Sefelnasr, A. A. Ebraheemand, and A. El-Shafie (2022). "Past, present and perspective methodology for groundwater modeling-based machine learning approaches". In: *Archives of Computational Methods in Engineering* 29.6, pp. 3843–3859. DOI: 10.1007/s11831-022-09715-w (cit. on p. 3).

Papacharalampous, G. and H. Tyralis (Oct. 2022). "A review of machine learning concepts and methods for addressing challenges in probabilistic hydrological post-processing and forecasting". In: *Frontiers in Water* 4. DOI: 10.3389/frwa.2022.961954. URL: https://doi.org/10.3389%2Ffrwa.2022.961954 (cit. on pp. 3, 4).

Papagiannopoulou, C., D. G. Miralles, S. Decubber, M. Demuzere, N. E. C. Verhoest, W. A. Dorigo, and W. Waegeman (2017). "A non-linear Granger-causality framework to investigate climate–vegetation dynamics". In: *Geoscientific Model Development* 10.5, pp. 1945–1960. DOI: 10.5194/gmd-10-1945-2017. URL: https://gmd.copernicus.org/articles/10/1945/2017/ (cit. on p. 10).

Patil, S. D. and M. Stieglitz (2015). "Comparing spatial and temporal transferability of hydrological model parameters". In: *Journal of Hydrology* 525, pp. 409–417. ISSN: 0022-1694. DOI: 10.1016/j.jhydrol.2015.04.003. URL: https://www.sciencedirect.com/science/article/pii/S0022169415002528 (cit. on p. 3).

Pedregosa, F., G. Varoquaux, A. Gramfort, V. Michel, B. Thirion, O. Grisel, M. Blondel, P. Prettenhofer, R. Weiss, V. Dubourg, J. Vanderplas, A. Passos, D. Cournapeau, M. Brucher, M. Perrot, and É. Duchesnay (2011). "Scikit-learn: Machine Learning in Python". In: *Journal of Machine Learning Research* 12.85, pp. 2825–2830. URL: http://jmlr.org/papers/v12/pedregosa11a.html (cit. on pp. 20, 24, 25).

Pekel, J.-F., A. Cottam, N. Gorelick, and A. Belward (Dec. 2016). "High-resolution mapping of global surface water and its long-term changes". In: *Nature* 540, pp. 418–422. DOI: 10.1038/nature20584 (cit. on pp. 2–4, 16, 41).

Picado, A., J. M. Dias, and A. B. Fortunato (2009). "Effect of flooding the salt pans in the Ria de Aveiro". In: *Journal of Coastal Research*, pp. 1395–1399. ISSN: 07490208, 15515036. URL: http://www.jstor.org/stable/25738018 (visited on 09/14/2023) (cit. on p. 1).

Prigent, C., F. Papa, F. Aires, W. B. Rossow, and E. Matthews (2007). "Global inundation dynamics inferred from multiple satellite observations, 1993–2000". In: *Journal of Geophysical Research: Atmospheres* 112.D12. DOI: 10.1029/2006JD007847. URL: https://agupubs.onlinelibrary.wiley.com/doi/abs/10.1029/2006JD007847 (cit. on pp. 2, 13, 18).

Probst, P., M. N. Wright, and A.-L. Boulesteix (Jan. 2019). "Hyperparameters and tuning strategies for random forest". In: *WIREs Data Mining and Knowledge Discovery* 9.3. DOI: 10.1002/widm.1301. URL: https://doi.org/10.1002%2Fwidm.1301 (cit. on pp. 20, 24).

Rebala, G., A. Ravi, and S. Churiwala (Jan. 2019). *An Introduction to Machine Learning*. ISBN: 978-3-030-15728-9. DOI: 10.1007/978-3-030-15729-6 (cit. on p. 25).

Rees, W. G. (2012). *Physical Principles of Remote Sensing*. 3rd ed. Cambridge, UK: Cambridge University Press. DOI: 10.1017/CBO9781139017411 (cit. on pp. 13, 14).

Reschke, J., A. Bartsch, S. Schlaffer, and D. Schepaschenko (2012). "Capability of C-Band SAR for Operational Wetland Monitoring at High Latitudes". In: *Remote Sensing* 4.10, pp. 2923–2943. ISSN: 2072-4292. DOI: 10.3390/rs4102923. URL: https://www.mdpi.com/2072-4292/4/10/2923 (cit. on pp. 2, 13, 18).

RH (2020). *Natonalpark Neusiedler See – Seewinkel Bericht des Rechnungshofes*. Tech. rep. 29. Rechnungshofs Österreich (cit. on p. 8).

Riley, J. W. and C. C. Stillwell (2023). "Predicting Inundation Dynamics and Hydroperiods of Small, Isolated Wetlands Using a Machine Learning Approach". In: *Wetlands* 43.6, p. 63. DOI: 10.1007/s13157-023-01706-2 (cit. on pp. 4, 20).

Ripley, B. D. (2007). *Pattern recognition and neural networks*. Cambridge university press (cit. on p. 21).

Rouse, J. W., R. H. Haas, J. A. Schell, D. W. Deering, et al. (1974). "Monitoring vegetation systems in the Great Plains with ERTS". In: *NASA Spec. Publ* 351.1, p. 309 (cit. on p. 16).

Saarela, M. and S. Jauhiainen (Feb. 2021). "Comparison of feature importance measures as explanations for classification models". In: *SN Applied Sciences* 3, pp. 1–12. DOI: 10.1007/s42452-021-04148-9 (cit. on pp. 20, 25).

Safaee, S. and J. Wang (2020). "Towards global mapping of salt pans and salt playas using Landsat imagery: a case study of western United States". In: *International Journal of Remote Sensing* 41.22, pp. 8693–8716. DOI: 10.1080/01431161.2020.1781285. URL: https://doi.org/10.1080%2F01431161.2020.1781285 (cit. on pp. 1, 2, 14).

Sakamoto, T., N. V. Nguyen, A. Kotera, H. Ohno, N. Ishitsuka, and M. Yokozawa (Aug. 2007). "Detecting temporal changes in the extent of annual flooding within the Cambodia and the Vietnamese Mekong Delta from MODIS time-series imagery". In: *Remote Sensing of Environment* 109.3, pp. 295–313. DOI: 10.1016/j.rse.2007.01.011. URL: https://doi.org/10.1016%2Fj.rse.2007.01.011 (cit. on p. 17).

Schaepman-Strub, G., M. Schaepman, T. Painter, S. Dangel, and J. Martonchik (July 2006). "Reflectance quantities in optical remote sensing—definitions and case studies". In: *Remote Sensing of Environment* 103.1, pp. 27–42. DOI: 10.1016/j.rse.2006.03.002. URL: https://doi.org/10.1016%2Fj.rse.2006.03.002 (cit. on p. 17).

Schauer, H., S. Schlaffer, E. Bueechi, and W. Dorigo (2023). "Inundation–Desiccation State Prediction for Salt Pans in the Western Pannonian Basin Using Remote Sensing, Groundwater, and Meteorological Data". In: *Remote Sensing* 15.19. ISSN: 2072-4292. DOI: 10.3390/rs15194659. URL: https://www.mdpi.com/2072-4292/15/19/4659 (cit. on pp. III, 8, 15, 17, 18, 27).

Schlaffer, S., M. Chini, W. Dorigo, and S. Plank (2022). "Monitoring surface water dynamics in the Prairie Pothole Region of North Dakota using dual-polarised Sentinel-1 synthetic aperture radar (SAR) time series". In: *Hydrology and Earth System Sciences* 26.3, pp. 841–860. DOI: 10.

5194/hess-26-841-2022. URL: https://hess.copernicus.org/articles/26/841/2022/ (cit. on pp. 2, 13, 18).

Schlaffer, S., M. Chini, D. Dettmering, and W. Wagner (2016). "Mapping Wetlands in Zambia Using Seasonal Backscatter Signatures Derived from ENVISAT ASAR Time Series". In: *Remote Sensing* 8 (5), p. 402. ISSN: 2072-4292. DOI: 10.3390/rs8050402. URL: http://doi.org/10.3390/rs8050402 (cit. on pp. 2, 13).

Schwatke, C., D. Dettmering, W. Bosch, and F. Seitz (2015). "DAHITI – an innovative approach for estimating water level time series over inland waters using multi-mission satellite altimetry". In: *Hydrology and Earth System Sciences* 19.10, pp. 4345–4364. DOI: 10.5194/hess-19-4345-2015. URL: https://hess.copernicus.org/articles/19/4345/2015/ (cit. on p. 18).

Secci, D., M. G. Tanda, M. D'Oria, V. Todaro, and C. Fagandini (2021). "Impacts of climate change on groundwater droughts by means of standardized indices and regional climate models". In: *Journal of Hydrology* 603, p. 127154. ISSN: 0022-1694. DOI: 10.1016/j.jhydrol.2021.127154. URL: https://www.sciencedirect.com/science/article/pii/S002216942101204X (cit. on p. 9).

Shaeri Karimi, S., N. Saintilan, L. Wen, and R. Valavi (2019). "Application of Machine Learning to Model Wetland Inundation Patterns Across a Large Semiarid Floodplain". In: *Water Resources Research* 55.11, pp. 8765–8778. DOI: 10.1029/2019WR024884. URL: https://agupubs.onlinelibrary.wiley.com/doi/abs/10.1029/2019WR024884 (cit. on pp. 4, 20).

Shahtahmassebi, A., N. Yang, K. Wang, N. Moore, and Z. Shen (2013). "Review of shadow detection and de-shadowing methods in remote sensing". In: *Chinese geographical science* 23, pp. 403–420 (cit. on p. 17).

Sharma, L., R. Naik, and P. Pandey (Apr. 2021). "A Focus on Reaggregation of Playa Wetlandscapes in the Face of Global Ecological Disconnectivity". In: pp. 366–387. ISBN: 9781119616016. DOI: 10.1002/9781119616016.ch18 (cit. on p. 1).

Shaw, P. and R. Bryant (2011). "Pans, Playas and Salt Lakes". In: *Arid Zone Geomorphology*. Hoboken, NJ, USA: John Wiley and Sons, Ltd. Chap. 15, pp. 373–401. ISBN: 9780470710777. DOI: 10.1002/9780470710777.ch15. URL: https://onlinelibrary.wiley.com/doi/abs/10.1002/9780470710777.ch15 (cit. on pp. 1, 2).

Shen, C., X. Chen, and E. Laloy (2021). *Editorial: Broadening the Use of Machine Learning in Hydrology, Frontiers in Water, 3* (cit. on p. 3).

Shen, L. and C. Li (2010). "Water body extraction from Landsat ETM+ imagery using adaboost algorithm". In: *2010 18th International Conference on Geoinformatics*. IEEE, pp. 1–4 (cit. on p. 17).

Sheng, Y., C. Song, J. Wang, E. A. Lyons, B. R. Knox, J. S. Cox, and F. Gao (Nov. 2016). "Representative lake water extent mapping at continental scales using multi-temporal Landsat-8 imagery". In: *Remote Sensing of Environment* 185, pp. 129–141. DOI: 10.1016/j.rse.2015.12.041. URL: https://doi.org/10.1016%2Fj.rse.2015.12.041 (cit. on p. 2).

Silva, M. F. da, H. Albuquerque, F. Martins, and G. Buron (Apr. 2022). "Salt pans: An Indissociable Natural and Cultural Heritage – A Comparative Study Between Aveiro, Portugal and Guérande, France". In: *Tourism Planning and Development in Western Europe*. Hoboken, NJ, USA: CABI, pp. 65–79. DOI: 10.1079/9781800620797.0005. URL: https://doi.org/10.1079%2F9781800620797.0005 (cit. on p. 1).

Sima, C. and E. R. Dougherty (July 2006). "What should be expected from feature selection in small-sample settings". In: *Bioinformatics* 22.19, pp. 2430–2436. ISSN: 1367-4803. DOI: 10.1093/bioinformatics/btl407 (cit. on p. 8).

Sit, M., B. Z. Demiray, Z. Xiang, G. J. Ewing, Y. Sermet, and I. Demir (Aug. 2020). "A comprehensive review of deep learning applications in hydrology and water resources". In: *Water*

Science and Technology 82.12, pp. 2635–2670. ISSN: 0273-1223. DOI: 10.2166/wst.2020.369. URL: https://doi.org/10.2166/wst.2020.369 (cit. on p. 4).

Sogno, P., I. Klein, and C. Kuenzer (May 2022). "Remote Sensing of Surface Water Dynamics in the Context of Global Change—A Review". In: *Remote Sensing* 14, p. 2475. DOI: 10.3390/rs14102475 (cit. on p. 4).

Soja, G., J. Züger, M. Knoflacher, P. Kinner, and A.-M. Soja (2013). "Climate impacts on water balance of a shallow steppe lake in Eastern Austria (Lake Neusiedl)". In: *Journal of Hydrology* 480, pp. 115–124. ISSN: 0022-1694. DOI: 10.1016/j.jhydrol.2012.12.013. URL: https://www.sciencedirect.com/science/article/pii/S0022169412010736 (cit. on p. 7).

Soltani, K., A. Amiri, M. Zeynoddin, I. Ebtehaj, B. Gharabaghi, and H. Bonakdari (2020). "Forecasting monthly fluctuations of lake surface areas using remote sensing techniques and novel Machine Learning Methods". In: *Theoretical and Applied Climatology* 143.1–2, pp. 713–735. DOI: 10.1007/s00704-020-03419-6 (cit. on p. 4).

Solvik, K., A. M. Bartuszevige, M. Bogaerts, and M. B. Joseph (Nov. 2021). "Predicting Playa Inundation Using a Long Short-Term Memory Neural Network". In: *Water Resources Research* 57.12. DOI: 10.1029/2020wr029009. URL: https://doi.org/10.1029%2F2020wr029009 (cit. on pp. 4, 20).

Sun, F., M. L. Roderick, and G. D. Farquhar (Feb. 2018). "Rainfall statistics, stationarity, and climate change". In: *Proceedings of the National Academy of Sciences* 115.10, pp. 2305–2310. DOI: 10.1073/pnas.1705349115. URL: https://doi.org/10.1073%2Fpnas.1705349115 (cit. on p. 40).

Tallaksen, L. M., H. Hisdal, and H. A. V. Lanen (2009). "Space–time modelling of catchment scale drought characteristics". In: *Journal of Hydrology* 375.3, pp. 363–372. ISSN: 0022-1694. DOI: 10.1016/j.jhydrol.2009.06.032 (cit. on p. 40).

team, T. pandas development (June 2023). *pandas-dev/pandas: Pandas*. Version v2.0.3. DOI: 10.5281/zenodo.8092754. (Visited on 08/10/2023) (cit. on pp. 10, 11).

Tolotti, M., G. Guella, A. Herzig, M. Rodeghiero, N. L. Rose, G. Soja, T. Zechmeister, H. Yang, and K. Teubner (2021). "Assessing the ecological vulnerability of the shallow steppe Lake Neusiedl (Austria-Hungary) to climate-driven hydrological changes using a palaeolimnological approach". In: *Journal of Great Lakes Research* 47.5, pp. 1327–1344. ISSN: 0380-1330. DOI: 10.1016/j.jglr.2021.06.004. URL: https://www.sciencedirect.com/science/article/pii/S0380133021001325 (cit. on p. 7).

Trabs, M., M. Jirak, K. Krenz, and M. Reiß (2021). *Statistik und maschinelles Lernen*. Springer Berlin Heidelberg. DOI: 10.1007/978-3-662-62938-3. URL: https://doi.org/10.1007%2F978-3-662-62938-3 (cit. on p. 19).

Turak, E., I. Harrison, D. Dudgeon, R. Abell, A. Bush, W. Darwall, C. M. Finlayson, S. Ferrier, J. Freyhof, V. Hermoso, et al. (2017). "Essential Biodiversity Variables for measuring change in global freshwater biodiversity". In: *Biological Conservation* 213, pp. 272–279. DOI: 10.1016/j.biocon.2016.09.005 (cit. on p. 2).

Turkeltaub, T. and G. Bel (2023). "The effects of rain and evapotranspiration statistics on groundwater recharge estimations for semi-arid environments". In: *Hydrology and Earth System Sciences* 27.1, pp. 289–302. DOI: 10.5194/hess-27-289-2023. URL: https://hess.copernicus.org/articles/27/289/2023/ (cit. on p. 9).

Tyralis, H., G. Papacharalampous, and A. Langousis (2019). "A Brief Review of Random Forests for Water Scientists and Practitioners and Their Recent History in Water Resources". In: *Water* 11.5. ISSN: 2073-4441. DOI: 10.3390/w11050910. URL: https://www.mdpi.com/2073-4441/11/5/910 (cit. on pp. 4, 19).

Ulaby, F. T., R. K. Moore, and A. K. Fung (1981). *Microwave remote sensing: Active and passive. volume 1-microwave remote sensing fundamentals and radiometry* (cit. on p. 18).

Vanderhoof, M. K., C. R. Lane, M. G. McManus, L. C. Alexander, and J. R. Christensen (2018). "Wetlands inform how climate extremes influence surface water expansion and contraction". In: *Hydrology and Earth System Sciences* 22.3, pp. 1851–1873. DOI: 10.5194/hess-22-1851-2018 (cit. on pp. 1, 40).

Vanderhoof, M., L. Alexander, and J. Todd (May 2016). "Temporal and spatial patterns of wetland extent influence variability of surface water connectivity in the Prairie Pothole Region, United States". In: *Landscape Ecology* 30. DOI: 10.1007/s10980-015-0290-5. URL: https://link.springer.com/article/10.1007/s10980-015-0290-5 (cit. on p. 41).

Vicente-Serrano, S. M., S. Beguería, and J. I. López-Moreno (2010). "A Multiscalar Drought Index Sensitive to Global Warming: The Standardized Precipitation Evapotranspiration Index". In: *Journal of Climate* 23.7, pp. 1696–1718. DOI: 10.1175/2009JCLI2909.1. URL: https://journals.ametsoc.org/view/journals/clim/23/7/2009jcli2909.1.xml (cit. on pp. 9, 11).

Vijayaraj, V., N. Younan, and C. O'Hara (2006). "Concepts of Image Fusion in Remote Sensing Applications". In: *2006 IEEE International Symposium on Geoscience and Remote Sensing*, pp. 3798–3801. DOI: 10.1109/IGARSS.2006.973 (cit. on p. 13).

Virtanen, P., R. Gommers, T. E. Oliphant, M. Haberland, T. Reddy, D. Cournapeau, E. Burovski, P. Peterson, W. Weckesser, J. Bright, S. J. van der Walt, M. Brett, J. Wilson, K. J. Millman, N. Mayorov, A. R. J. Nelson, E. Jones, R. Kern, E. Larson, C. J. Carey, İ. Polat, Y. Feng, E. W. Moore, J. VanderPlas, D. Laxalde, J. Perktold, R. Cimrman, I. Henriksen, E. A. Quintero, C. R. Harris, A. M. Archibald, A. H. Ribeiro, F. Pedregosa, P. van Mulbregt, and SciPy 1.0 Contributors (2020). "SciPy 1.0: Fundamental Algorithms for Scientific Computing in Python". In: *Nature Methods* 17, pp. 261–272. DOI: 10.1038/s41592-019-0686-2 (cit. on p. 19).

Waskom, M. L. (2021). "seaborn: statistical data visualization". In: *Journal of Open Source Software* 6.60, p. 3021. DOI: 10.21105/joss.03021. URL: 10.21105/joss.03021 (cit. on p. 19).

Wasserman, J., J. B. Adams, and D. A. Lemley (2022). "Investigating the potential for saltpan restoration for the provision of multiple ecosystem services". In: *African Journal of Aquatic Science* 47.4, pp. 436–446. DOI: 10.2989/16085914.2022.2067823. URL: https://doi.org/10.2989/16085914.2022.2067823 (cit. on p. 1).

Wee, W. J., N. B. Zaini, A. N. Ahmed, and A. El-Shafie (2021). "A review of models for water level forecasting based on machine learning". In: *Earth Science Informatics* 14.4, pp. 1707–1728. DOI: 10.1007/s12145-021-00664-9 (cit. on p. 4).

Wezernak, C. T., R. E. Turner, and D. Lyzenga (1976). *Spectral reflectance and radiance characteristics of water pollutants*. Tech. rep. NASA (cit. on p. 13).

Williams, D. D. (2006). *The biology of temporary waters*. Oxford University Press, USA (cit. on p. 2).

Williams, W. D. (2004). "Lakes in Arid Environments". In: *The Lakes Handbook*. Oxford, UK: John Wiley Sons, Ltd. Chap. 8, pp. 200–240. ISBN: 9780470750506. DOI: 10.1002/9780470750506.ch8. URL: https://onlinelibrary.wiley.com/doi/abs/10.1002/9780470750506.ch8 (cit. on p. 1).

WMO (2017). *WMO Guidelines on the Calculation of Climate Normals*. Tech. rep. (cit. on p. 9).

Wong, T.-T. (2015). "Performance evaluation of classification algorithms by k-fold and leave-one-out cross validation". In: *Pattern Recognition* 48.9, pp. 2839–2846. ISSN: 0031-3203. DOI: 10.1016/j.patcog.2015.03.009 (cit. on pp. 22, 25).

Wulder, M. A., J. C. White, T. R. Loveland, C. E. Woodcock, A. S. Belward, W. B. Cohen, E. A. Fosnight, J. Shaw, J. G. Masek, and D. P. Roy (2016). "The global Landsat archive:

Status, consolidation, and direction". In: *Remote Sensing of Environment* 185, pp. 271–283 (cit. on p. 4).

Wulder, M. A., T. R. Loveland, D. P. Roy, C. J. Crawford, J. G. Masek, C. E. Woodcock, R. G. Allen, M. C. Anderson, A. S. Belward, W. B. Cohen, J. Dwyer, A. Erb, F. Gao, P. Griffiths, D. Helder, T. Hermosilla, J. D. Hipple, P. Hostert, M. J. Hughes, J. Huntington, D. M. Johnson, R. Kennedy, A. Kilic, Z. Li, L. Lymburner, J. McCorkel, N. Pahlevan, T. A. Scambos, C. Schaaf, J. R. Schott, Y. Sheng, J. Storey, E. Vermote, J. Vogelmann, J. C. White, R. H. Wynne, and Z. Zhu (2019). "Current status of Landsat program, science, and applications". In: *Remote Sensing of Environment* 225, pp. 127–147. ISSN: 0034-4257. DOI: 10.1016/j.rse.2019.02.015. URL: https://www.sciencedirect.com/science/article/pii/S0034425719300707 (cit. on pp. 2, 4).

Wulder, M. A., D. P. Roy, V. C. Radeloff, T. R. Loveland, M. C. Anderson, D. M. Johnson, S. Healey, Z. Zhu, T. A. Scambos, N. Pahlevan, M. Hansen, N. Gorelick, C. J. Crawford, J. G. Masek, T. Hermosilla, J. C. White, A. S. Belward, C. Schaaf, C. E. Woodcock, J. L. Huntington, L. Lymburner, P. Hostert, F. Gao, A. Lyapustin, J.-F. Pekel, P. Strobl, and B. D. Cook (2022). "Fifty years of Landsat science and impacts". In: *Remote Sensing of Environment* 280, p. 113195. ISSN: 0034-4257. DOI: 10.1016/j.rse.2022.113195. URL: https://www.sciencedirect.com/science/article/pii/S0034425722003054 (cit. on p. 14).

Wurtsbaugh, W. A., C. Miller, S. E. Null, R. J. DeRose, P. Wilcock, M. Hahnenberger, F. Howe, and J. Moore (2017). "Decline of the world's saline lakes". In: *Nature Geoscience* 10.11, pp. 816–821. DOI: 10.1038/ngeo3052 (cit. on p. 1).

Xu, H. (2006). "Modification of normalised difference water index (NDWI) to enhance open water features in remotely sensed imagery". In: *International Journal of Remote Sensing* 27.14, pp. 3025–3033. DOI: 10.1080/01431160600589179. URL: 10.1080/01431160600589179 (cit. on pp. 16, 17).

Xu, T. and F. Liang (2021). "Machine learning for hydrologic sciences: An introductory overview". In: *WIREs Water* 8.5, e1533. DOI: 10.1002/wat2.1533. URL: https://wires.onlinelibrary.wiley.com/doi/abs/10.1002/wat2.1533 (cit. on pp. 3, 4).

Xu, Y. and R. Goodacre (2018). "On splitting training and validation set: a comparative study of cross-validation, bootstrap and systematic sampling for estimating the generalization performance of supervised learning". In: *Journal of Analysis and Testing* 2.3, pp. 249–262. DOI: 10.1007/s41664-018-0068-2 (cit. on p. 21).

Yang, W., R. Xia, H. Chen, M. Wang, and C.-Y. Xu (2022). "The impact of calibration conditions on the transferability of conceptual hydrological models under stationary and nonstationary climatic conditions". In: *Journal of Hydrology* 613, p. 128310. ISSN: 0022-1694. DOI: 10.1016/j.jhydrol.2022.128310. URL: https://www.sciencedirect.com/science/article/pii/S0022169422008824 (cit. on p. 3).

Zhai, H., H. Zhang, L. Zhang, and P. Li (2018). "Cloud/shadow detection based on spectral indices for multi/hyperspectral optical remote sensing imagery". In: *ISPRS Journal of Photogrammetry and Remote Sensing* 144, pp. 235–253. ISSN: 0924-2716. DOI: 10.1016/j.isprsjprs.2018.07.006. URL: https://www.sciencedirect.com/science/article/pii/S0924271618301989 (cit. on p. 17).

Zhu, Q. (2020). "On the performance of Matthews correlation coefficient (MCC) for imbalanced dataset". In: *Pattern Recognition Letters* 136, pp. 71–80. ISSN: 0167-8655. DOI: 10.1016/j.patrec.2020.03.030 (cit. on p. 25).

Zhu, S., H. Lu, M. Ptak, J. Dai, and Q. Ji (2020). "Lake water-level fluctuation forecasting using machine learning models: a systematic review". In: *Environmental Science and Pollution Research* 27.36, pp. 44807–44819. DOI: 10.1007/s11356-020-10917-7 (cit. on p. 4).

Zimmermann-Timm, H. and K. Teubner (2021). "Folgen der Grundwassersenkung am Beispiel des Neusiedlers See Seewinkel (Burgenland, Österreich)". In: *Warnsignal Klima: Boden und Landnutzung*. Ed. by H. G. Lozán J. L. S.-W. Breckle and D. Kasang. Oxford: Wissenschaftliche Auswertungen in Kooperation mit GEO, pp. 142–149. DOI: DOI:10.25592/warnsignal.klima.boden-landnutzung.19 (cit. on pp. 1, 2, 7–10, 15, 19, 39, 41, 42, 45).

Zounemat-Kermani, M., O. Batelaan, M. Fadaee, and R. Hinkelmann (2021). "Ensemble machine learning paradigms in hydrology: A review". In: *Journal of Hydrology* 598, p. 126266. ISSN: 0022-1694. DOI: 10.1016/j.jhydrol.2021.126266. URL: https://www.sciencedirect.com/science/article/pii/S0022169421003139 (cit. on pp. 3, 19).